Glial Nrf2 signaling mediates the neuroprotection exerted by *Gastrodia elata* Blume in Lrrk2-G2019S Parkinson's disease

Yu-En Lin[1,2], Chin-Hsien Lin[3], En-Peng Ho[3], Yi-Ci Ke[3], Stavroula Petridi[4,5], Christopher J. H. Elliott[4], Lee-Yan Sheen[2,*], and Cheng-Ting Chien[1,6,*]

[1]Institute of Molecular Biology, Academia Sinica, Taipei, Taiwan

[2]Institute of Food Science and Technology, National Taiwan University, Taipei, Taiwan

[3]Department of Neurology, National Taiwan University Hospital, Taipei, Taiwan

[4]Department of Biology and York Biomedical Research Institute, University of York, York, UK

[5]Department of Clinical Neurosciences and MRC Mitochondrial Biology Unit, University of Cambridge, Cambridge CB2 0XY, UK

[6]Neuroscience Program of Academia Sinica, Academia Sinica, Taipei, Taiwan

*Correspondence:

Lee-Yan Sheen, E-mail: lysheen@ntu.edu.tw, Tel.: +886-2-3366-1572

Cheng-Ting Chien, E-mail: ctchien@gate.sinica.edu.tw, Tel.: +886-2-2789-9970

Abstract

The most frequent missense mutations in familial Parkinson's disease (PD) occur in the highly conserved *LRRK2/PARK8* gene with G2019S mutation. We previously established a fly model of PD carrying the *LRRK2-G2019S* mutation that exhibited the parkinsonism-like phenotypes. An herbal medicine—*Gastrodia elata* Blume (GE), has been reported to have neuroprotective effects in toxin-induced PD models. However, the underpinning molecular mechanisms of GE beneficiary to G2019S-induced PD remain unclear. Here, we show that these G2019S flies treated with water extracts of GE (WGE) and its bioactive compounds, gastrodin and 4-HBA, displayed locomotion improvement and dopaminergic neuron protection. WGE suppressed the accumulation and hyperactivation of G2019S proteins in dopaminergic neurons, and activated the antioxidation and detoxification factor Nrf2 mostly in the astrocyte-like and ensheathing glia. Glial activation of Nrf2 antagonizes G2019S-induced Mad/Smad signaling. Moreover, we treated *LRRK2-G2019S* transgenic mice with WGE and found the locomotion declines, the loss of dopaminergic neurons, and the number of hyperactive microglia were restored. WGE also suppressed the hyperactivation of G2019S proteins and regulated the Smad2/3 pathways in the mice brains. We conclude that WGE prevents locomotion defects and the neuronal loss induced by G2019S mutation via glial Nrf2/Mad signaling, unveiling a potential therapeutic avenue for PD.

Introduction

Parkinson's disease (PD) is a highly prevalent neurodegenerative disorder characterized by the loss of dopaminergic neurons in the substantia nigra projecting to the striatum of the basal ganglion, representing a circuit involved in motor planning and coordination. As a consequence, PD is associated with motor abnormalities, bradykinesia, hypokinesia, rigidity and resting tremor. Currently, the most frequently applied pharmacological treatment, levodopa (L-DOPA), exerts limited motor improvement and elicits negative side-effects (Ray Chaudhuri et al., 2018). Hence, identifying and developing alternative or complementary treatments may assist in mitigating PD progression.

PD is a multi-causal disease with a complicated etiology, including familial inheritance. More than 20 *PARK* genes have been genetically linked to PD, a number that is increasing (Houlden & Singleton, 2012). Missense mutations in *PARK8*, or *Leucine-rich repeat kinase 2* (*LRRK2*) induce characteristic PD symptoms and pathologies such as loss of dopaminergic neurons and the appearance of Lewy bodies (Martin et al., 2014). Notably, the most commonly observed mutation, dominant G2019S, among familial PD cases is located in the kinase domain of Lrrk2, which augments its kinase activity via auto- and hyper-activation (Sheng et al., 2012). The hyperactive G2019S mutant protein alters several cellular processes, including vesicle trafficking, microtubule dynamics, autophagy, mitochondrial function (Martin et al., 2014), and most commonly, increases susceptibility to oxidative stress that contributes to neuronal degeneration (Angeles et al., 2011; Nguyen et al., 2011). These indicate that regulation of the hyperactivation of G2019S mutant protein appears to be a disease-modifying strategy.

Glia provide structural and metabolic supports to neurons and regulate synaptic transmissions, so they are important for the function and survival of dopaminergic neurons (Lin et al., 1993; Sofroniew & Vinters, 2010). Dysfunction in two major glial types, astrocytes and microglia, contribute to the onset and progression of both sporadic and familial PD (Kam et al., 2020). Astrocytes and microglia of postmortem PD brains exhibit pathologic lesions and hyper-immunoactivity (Miklossy et al., 2006). A clinical trial involving down-regulation of microglial oxidative stress highlights the significance of glia to PD (Jucaite et al., 2015). Moreover, Lrrk2 regulates the inflammatory response in microglia and the autophagy-

61 lysosome pathway in astrocytes, with the G2019S mutation altering the size and pH of lysosomes (Henry
62 et al., 2015; Moehle et al., 2012). Expression of G2019S mutant protein in neurons was previously shown
63 to induce the secretion of Glass bottom boat (Gbb)/bone morphogenetic protein (BMP) signal that, in
64 turn, upregulates Mothers against decapentaplegic (Mad)/Smad signaling in glia, which prompts feedback
65 signals to promote neuronal degeneration (Maksoud et al., 2019). These studies indicate that G2019S
66 mutant protein alters the homeostasis and interaction between neurons and glia, contributing to PD
67 pathogenesis. However, whether any dietary or pharmacological treatment blockading this neuron-glia
68 interaction beneficiary to G2019S-induced PD is unclear.

69 Given that up to 70% of human *PARK* genes are conserved in the *Drosophila* genome, *Drosophila* is
70 frequently used as a PD model for studying gene function, such as the *PARK1/SNCA* (Chen & Feany,
71 2005) and *PARK8/LRRK2* (Liu et al., 2008). Genetic and molecular linkage between *PINK1/PARK6* and
72 *Parkin/PARK2* was first established in *Drosophila* (Clark et al., 2006). When overexpressed in
73 *Drosophila* dopaminergic neurons, *LRRK2* transgenes carrying G2019S or other dominant mutations
74 induce dopaminergic neuron loss and locomotion impairment, two age-dependent symptoms of PD (Lin
75 et al., 2010; Liu et al., 2008). The G2019S model has further been used to screen a collection of FDA-
76 approved drugs to suppress these PD phenotypes. Thus, *Drosophila* represents an amenable model of PD
77 for genetic, molecular and pharmacological study of potential therapeutic interventions. Strikingly,
78 lovastatin was found to prevent dendrite degeneration, dopaminergic neuron loss, and impaired
79 locomotion and, critically, a lovastatin-involved Nrf2 pathway proved neuroprotective (C. H. Lin et al.,
80 2016). Nevertheless, whether the Nrf2-mediated neuroprotection is cell- or non-cell-autonomous,
81 remaining elusive.

82 Traditional Chinese Medicine (TCM) is often used as an alternative or dietary treatment for human
83 diseases, including PD (Kim et al., 2012; Li et al., 2017). Although the results were inconclusive, some
84 TCM could display adjuvant effects when used in combination with L-DOPA, reducing the L-DOPA
85 dosage required in long-term treatments and relieving non-motor symptoms (Kim et al., 2012). As a
86 prominent component in TCM, *Gastrodia elata* Blume (GE; Orchidaceae) has been used to treat

87 neurological disorders for centuries (Chen & Sheen, 2011). GE has been shown to exert neuroprotective,
88 anti-inflammatory and antioxidative effects in neurodegenerative disease models (Jang et al., 2015). The
89 major bioactive compounds in GE include gastrodin and 4-hydroxybenzyl alcohol (4-HBA), both of
90 which display pharmacological effects on neurobiological and psychological disorders (Chen et al., 2016;
91 Kumar et al., 2013). Additionally, gastrodin and 4-HBA have been reported to activate the Nrf2 signaling
92 in dopaminergic neurons and astrocytes, respectively (Jiang et al., 2014; Luo et al., 2017), highlighting a
93 potential benefit of incorporating GE in PD treatments. However, the effects and mechanisms underlying
94 how GE moderate Lrrk2-G2019S PD remain unclear.

95 In the present study, we treated G2019S animals with water extract of GE (WGE), and its bioactive
96 compounds, gastrodin and 4-HBA. We have investigated the impact of WGE treatment on PD in restoring
97 locomotion and protecting dopaminergic neurons in the *Drosophila* G2019S model. We identified two
98 distinct pathways induced by WGE in the model, i.e., suppression of Lrrk2 protein accumulation and
99 hyperphosphorylation in neurons, and activation of the Nrf2 pathway in glia, particularly in astrocyte-like
100 and ensheathing glia. We show that WGE-induced Nrf2 activation antagonizes the Gbb-activated Mad
101 signaling in glia, contributing to neuronal protection. WGE also suppressed the hyperactivation of
102 G2019S proteins and antagonized Smad2/3 signaling in a *LRRK2-G2019S* mouse model, which restored
103 locomotion, protected dopaminergic neurons and regulated the microglia hyperactivation. Conservation
104 of the pathways impacted by WGE treatment in both the *Drosophila* and mouse G2019S models implies
105 that the beneficial effects of GE and represent a reliable and effective complementary therapy for PD.
106

107 **Results**

108 **WGE treatment improves locomotion of *Ddc>G2019S* flies**

109 We employed the *GAL4-UAS* system to express the human G2019S mutant of Lrrk2 by the *Ddc-*
110 *GAL4* driver (*Ddc>G2019S*) in dopaminergic neurons and then assessed the anti-geotactic climbing
111 activity of adult flies. We observed that locomotion of *Ddc>G2019S* flies was affected significantly
112 relative to control flies expressing human wild-type Lrrk2 (*Ddc>Lrrk2*) (Figure 1A and Figure 1-figure
113 supplement 1A). At weeks 1 and 2, more than 80% of *Ddc>G2019S* flies could successfully climb above
114 an 8-cm threshold, a proportion comparable to that of *Ddc>Lrrk2* flies. However, the success rate
115 declined to ~40% at week 3, ~20% at week 4, and to less than 10% at weeks 5 and 6. These proportions
116 are significantly lower than the ~80% at week 3, ~60% at week 4, and ~40% at weeks 5 and 6 displayed
117 by *Ddc>Lrrk2* flies. Although both *Ddc>G2019S* and *Ddc>Lrrk2* flies failed to reach the 8-cm mark at
118 weeks 7 and 8, *Ddc>Lrrk2* flies could still climb the wall, whereas almost all *Ddc>G2019S* flies could
119 not (Figure 1-figure supplement 1A). We also tested the climbing activity of another control expressing
120 GFP in dopaminergic neurons (*Ddc>mCD8-GFP*). Both *Ddc>Lrrk2* and *Ddc>mCD8-GFP* flies showed
121 comparable climbing activities in the first six weeks, and a significant number of *Ddc>mCD8-GFP* flies
122 were still able to climb above the 8-cm mark at week 7. Therefore, we used the *Ddc>Lrrk2* line as a
123 control for *Ddc>G2019S* flies in subsequent experiments to dissect the specific mode of pathogenicity of
124 the G2019S mutation.

125 Next, we examined the effect of feeding flies with water extracts of GE (WGE) as a dietary
126 supplement at different concentrations (0.1, 0.5 or 1.0%, w/w). WGE treatment of *Ddc>G2019S* flies at
127 all three doses elicited a significant improvement in their climbing ability (Figure 1A). Strikingly, the
128 lowest concentration (0.1%) of WGE proved the most effective, with *Ddc>G2019S* flies still performing
129 well at climbing (i.e., comparably to *Ddc>Lrrk2* control flies) in weeks 5 and 6. The higher doses of
130 WGE (0.5 % and 1.0%) still exerted beneficial effects at weeks 3 and 4, albeit not as significantly as the
131 0.1% dose, but had no beneficial effect in weeks 5 and 6. As 0.1% is the lowest among the three doses
132 tested, we lowered the dose of WGE to 0.02% and found that 0.02% WGE was less effective than 0.1%

133 starting at week 3 till week 6, suggesting that 0.1% is the optimal does in restoring the climbing activity
134 of *Ddc>G2019S* flies (Figure 1-figure supplement 1B).

135 Gastrodin and 4-HBA are two major phenolic compounds in GE displaying neuropharmacological
136 effects (Zhan et al., 2016). Feeding *Ddc>G2019S* flies with food containing gastrodin (0.1 mM)
137 equivalent to the amount in 0.1% WGE also restored locomotion of *Ddc>G2019S* flies in weeks 2-4,
138 though its impact diminished to non-significant levels at weeks 5 and 6. However, increasing the
139 gastrodin dose ten-fold (1.0 mM) resulted in improved climbing activity at weeks 5 and 6 (Figure 1B).
140 Similarly, the equivalent 0.1 mM of 4-HBA, the aglyconic form of gastrodin and the bioactive form in the
141 brain (Wu et al., 2017), was sufficient to restore the climbing ability of *Ddc>G2019S* flies, and a ten-fold
142 dose at 1.0 mM had an even better effect (Figure 1C). These results indicate that both gastrodin and 4-
143 HBA are primary bioactive compounds in GE that prevent locomotion decline in *Ddc>G2019S* flies, and
144 higher doses are more beneficial to reach the effect as WGE did.

145 Success in the anti-gravity wall-climbing assay also requires an immediate response to startle
146 knockdown. Accordingly, we performed a second assay, free-walking in an open arena, to assess
147 improved locomotion. Consistently, free-walking by *Ddc>G2019S* flies was greatly impaired, with total
148 walking distance reduced to less than 20% that displayed by control *Ddc>Lrrk2* flies (Figure 1D).
149 Moreover, *Ddc>G2019S* flies displayed centrophobism, i.e., they avoided walking into the central open
150 space. Strikingly, 0.1% WGE feeding greatly extended walking distance and suppressed the
151 centrophobism of *Ddc>G2019S* flies. Together, these two assays strongly indicate that the defective
152 locomotion exhibited by *Ddc>G2019S* flies is greatly improved by feeding them with 0.1% WGE.
153 Because the improvement on the locomotion was more effective in flies fed with 0.1% WGE than the
154 pure compounds, we therefore fed the flies with 0.1% WGE in the following experiments.

155

156 **WGE treatment suppresses dopaminergic neuron loss in *Ddc>G2019S* brain**

157 Expression of G2019S mutant protein has been shown to induce a gradual loss of dopaminergic
158 neurons in the adult fly brain, contributing to impaired locomotion (Lin et al., 2010; Liu et al., 2008).

159 Several clusters of dopaminergic neurons have been identified in the adult brain of *Drosophila*. Here, we
160 focused on the PPL1, PPL2, PPM1/2 and PPM3 clusters that have well-defined roles in modulating
161 locomotion (Mao & Davis, 2009) to assess the effect of WGE treatment. We detected reduced numbers of
162 dopaminergic neurons in the PPL1, PPL2, PPM1/2, and PPM3 clusters of *Ddc>G2019S* flies relative to
163 *Ddc>Lrrk2* controls, which increased in severity from week 2 to 6 (Figure 2 and Figure 2-figure
164 supplement 1A to C). Consistently, feeding *Ddc>G2019S* flies with 0.1% WGE restored numbers of
165 dopaminergic neurons in these clusters to the levels observed in controls (Figure 2 and Figure 2-figure
166 supplement 1A to C). Thus, concomitant rescue of locomotion and dopaminergic neuron populations in
167 *Ddc>G2019S* flies indicates that WGE treatment likely promotes dopaminergic neuron survival to restore
168 locomotion.
169

170 **WGE treatment suppresses G2019S-induced Lrrk2 hyperactivation**

171 The enhanced survival of dopaminergic neurons due to WGE treatment implies that WGE induces
172 neuroprotective mechanisms in *Ddc>G2019S* flies. The G2019S mutation causes Lrrk2
173 hyperphosphorylation, protein accumulation, and aberrant cellular signaling (Price et al., 2018). Therefore,
174 we explored if WGE-induced neuroprotection is responsible for abrogating these processes in G2019S
175 flies. We detected comparable levels of Lrrk2 proteins in newly eclosed adult brains pan-neuronally
176 expressing wild-type Lrrk2 (*elav>Lrrk2*) or G2019S mutant protein (*elav>G2019S*) (Figure 3A).
177 However, phosphorylation levels at the Ser^{1292} autophosphorylation site was higher in the *elav>G2019S*
178 flies compared to *elav>Lrrk2* (Figure 3A and B). This outcome was also observed at week 4 (Figure 3F
179 and G), consistent with the idea that Lrrk2 is hyperactivated upon G2019S mutation.
180 Hyperphosphorylation in *elav>G2019S* flies led to Lrrk2 protein accumulation, as determined by total
181 Lrrk2 levels at weeks 2 and 4 (Figure 3D and E). However, both hyperphosphorylation and protein
182 accumulation were suppressed upon feeding *elav>G2019S* flies with 0.1% WGE (Figure 3D to G). In the
183 *elav>Lrrk2* control, WGE feeding had no effect on levels of wild-type Lrrk2 or Ser^{1292} phosphorylation
184 (Figure 3-figure supplement 1A to C). We further examined the G2019S mutant-activated downstream

185 effector Rab10, the phosphorylation status of which can serve as an indicator of Lrrk2 kinase activity
186 (Karayel et al., 2020). We observed that levels of phosphorylated Rab10 were increased in *elav>G2019S*
187 flies, but this phenotype was suppressed by WGE feeding (Figure 3F and H). Hence, feeding flies with
188 WGE suppresses G2019S-induced Lrrk2 protein phosphorylation, accumulation, and signaling.
189

190 **WGE treatment restores Akt/GSK3β/Nrf2 pathway activity**

191 The Akt/GSK3β/Nrf2 signaling axis has been shown to promote survival of dopaminergic neurons
192 and ameliorate motor dysfunction in PD models (C. H. Lin et al., 2016). We assayed the phosphorylation
193 status of Akt at Ser^{505} in newly eclosed adult fly head extracts and found reduced levels of pAkt in
194 *elav>G2019S* flies relative to *elav>Lrrk2* controls (Figure 3A and C). This pAkt reduction persisted at
195 weeks 2 and 4, but was abrogated by feeding *elav>G2019S* flies with 0.1% WGE (Figure 4A and B). We
196 also examined phosphorylation levels of Nrf2 at Ser^{40} and GSK3β at Ser^{9}, both of which were reduced
197 upon expression of G2019S mutant protein and were equally offset by WGE feeding (Figure 4C and D).
198 Induction of Akt/GSK3β/Nrf2 signaling activates expression of heme oxygenase 1 (HO-1), and we
199 observed diminished levels of this latter protein in *elav>G2019S* flies, which could be rescued by WGE
200 feeding (Figure 4C and D). Therefore, WGE feeding restores the Akt/GSK3β/Nrf2 signaling activity
201 compromised by the G2019S mutation.
202

203 **Glial Nrf2 mediates the beneficial effect of WGE on restored locomotion and neuronal protection in**
204 **G2019S flies**

205 Restoration of Akt/GSK3β/Nrf2 signaling activity by WGE treatment prompted us to test by genetic
206 assays if that signaling pathway mediates the WGE mode of action. We focused on the downstream
207 effector Nrf2 encoded by *cap-n-collar* (*cnc*) in *Drosophila*. Intriguingly, neither overexpression (*UAS-*
208 *cncC-FL2*) nor RNAi knockdown (*UAS-cncTRiP*) of Nrf2 in dopaminergic neurons had an impact on the
209 climbing ability of *Ddc>G2019S* flies (Figure 5A). Also, WGE feeding still rescued locomotion of
210 *Ddc>G2019S* flies with Nrf2 knockdown (*Ddc>G2019S; cncTRiP*) to levels comparable to WGE-fed

211 control flies (*Ddc>G2019S; mCD8-GFP*) without Nrf2 knockdown (Figure 5A). Thus, the Nrf2 pathway
212 activation by WGE that appears to be effective in protecting neurons and restoring locomotion is likely
213 exerted in cells other than neurons.

214 Nrf2 activation may be examined by assessing GFP signal from the *ARE-GFP* reporter that harbors
215 Nrf2 binding sites and responds to Nrf2 activation (Chatterjee & Bohmann, 2012). *ARE-GFP* adult fly
216 brains displayed low basal GFP signals (Figure 5C), but feeding with 0.1% WGE elicited many GFP-
217 positive signals in Repo-positive glia (arrowheads in Figure 5D), evidencing that glia may be the primary
218 cell type in which Nrf2 is activated.

219 Next, we investigated if WGE-induced Nrf2 activity in glia is effective in promoting locomotion in
220 G2019S flies. To this end, we employed the *LexA-LexAop* system to overexpress wild-type Lrrk2 or
221 G2019S mutant protein in dopaminergic neurons (*Ddc-LexA>Lrrk2* and *Ddc-LexA>G2019S*,
222 respectively), and used the *GAL4* driver to manipulate Nrf2/CncC activity in glia (*repo>cncC-FL2* for
223 overexpression and *repo>cnc-RNAi* for knockdown). As a first step, we validated the age-dependent
224 locomotion decline of *Ddc-LexA>G2019S* flies that was severer than *Ddc-LexA>Lrrk2* and could be
225 rescued by 0.1% WGE feeding (Figure 5-figure supplement 1). We then assayed the climbing ability of
226 *Ddc-LexA>G2019S* flies exhibiting *repo-GAL4*-driven Nrf2 overexpression in glia (*Ddc-LexA>G2019S;*
227 *repo>cncC-FL2*). Significantly, the *Ddc-LexA>G2019S; repo>cncC-FL2* flies performed better in the
228 climbing assay than *Ddc-LexA>G2019S; repo-GAL4* without Nrf2 overexpression (Figure 5B). We also
229 performed Nrf2 knockdown in glia (*Ddc-LexA>G2019S; repo>cnc-RNAi*), which had little impact on the
230 already declined climbing activity in *Ddc-LexA>G2019S; repo-GAL4* (Figure 5B). Importantly, WGE
231 feeding could not rescue locomotion deficits of glial Nrf2-knockdown flies (*Ddc-LexA>G2019S;*
232 *repo>cnc-RNAi*) (Figure 5B, compare to *Ddc-LexA>G2019S; repo-GAL4* with WGE feeding). Thus,
233 glial overexpression of Nrf2 partially restores locomotion of *Ddc-LexA>G2019S* flies, and glial depletion
234 of Nrf2 abolishes the ability of WGE to rescue impaired locomotion.

235 We stained dopaminergic neurons of 6-week-old adult fly brains and confirmed that numbers of TH-
236 positive dopaminergic neurons in the PPL1 cluster were reduced in the *Ddc-LexA>G2019S; repo-GAL4*

237 flies compared to *Ddc-LexA>Lrrk2*; *repo-GAL4* controls (Figure 5E and F). Importantly, numbers of
238 dopaminergic neurons in the PPL1 cluster were restored upon glial overexpression of Nrf2 in the *Ddc-*
239 *LexA>G2019*S; *repo>cncC-FL2* flies. In contrast, glial Nrf2 knockdown had little impact on the already
240 reduced dopaminergic neurons. Taken together, these results support that glial Nrf2 is compromised in
241 *Ddc-LexA>G2019S* flies, and glial expression of Nrf2 protects the dopaminergic neurons.

242 Although WGE feeding suppressed hyperactivity of G2019S mutant protein (Figure 3D to G), it was
243 not clear if WGE-mediated Nrf2 activation in glia could directly suppress mutant protein hyperactivity in
244 dopaminergic neurons. To test this possibility, we compared the levels of total Lrrk2 protein and
245 phosphorylated Lrrk2 protein in *Ddc-LexA>G2019S* with and without glial Nrf2 overexpression (*Ddc-*
246 *LexA>G2019S; repo-GAL4* and *Ddc-LexA>G2019S; repo>cncC*). We observed comparable levels of
247 Lrrk2 and pLrrk2 in the control and Nrf2 overexpression lines (Figure 6-figure supplement 1A to C).
248 Thus, the neuroprotective effects of Nrf2 activity are unlikely to operate through modulation of Lrrk2
249 levels or activity.

250

251 **Nrf2 in astrocyte-like and ensheathing glia are the major targets of WGE that alleviate *Lrrk2-***
252 ***G2019S* locomotion deficits**

253 Five types of glia with different morphologies and functions have been identified in the fly brain
254 (Freeman, 2015). We decided to identify specific subtypes of glia that may mediate the WGE-induced
255 Nrf2 activity endowing neuronal protection, given that dysfunctional astrocytes and microglia have been
256 linked to onset and progression of both sporadic and familial PD (Kam et al., 2020). In *Ddc-*
257 *LexA>G2019S* flies, *GAL4*-driven *cnc* knockdown in astrocyte-like (*Ddc-LexA>G2019S; alrm>cnc-*
258 *RNAi*) or ensheathing glia (*Ddc-LexA>G2019S; R56F03>cnc-RNAi*) abolished the improved locomotion
259 elicited by WGE treatment, recapitulating the effect of pan-glial Nrf2 knockdown (*Ddc-LexA>G2019S;*
260 *repo>cnc-RNAi*) (Figure 6A). This outcome was not observed when we used GAL4 drivers to knock
261 down *cnc* in cortex (*np2222*), perineurial (*np6293*), or subperineurial (*moody*) glia. We confirmed the
262 involvement of astrocyte-like and ensheathing glia by means of Nrf2 overexpression in astrocyte-like

263 (*Ddc-LexA>G2019S; alrm>cncC-FL2*) or ensheathing (*Ddc-LexA>G2019S; R56F03>cncC-FL2*) glia,
264 with both treatments improving the climbing activity of *Ddc-LexA>G2019S* flies not subjected to WGE
265 feeding (Figure 6B). These analyses indicate that WGE feeding induces Nrf2 activity in astrocyte-like
266 and ensheathing glia, which mitigates the reduced locomotion displayed by G2019S mutant-expressing
267 flies.

268 Next, we assayed Nrf2-regulated *ARE-GFP* expression in astrocyte-like and ensheathing glia of flies
269 expressing G2019S mutant protein and subjected to WGE treatment. We focused on the astrocyte-like
270 and ensheathing cells located adjacent to dopaminergic neurons. In control flies expressing wild-type
271 Lrrk2, we detected basal levels of GFP signal in mCherry-positive astrocyte-like (*alrm-GAL4*) or
272 ensheathing glia (*R56F03*) (Figure 6C to F). We detected lower levels of GFP signal in these cells when
273 G2019S mutant protein was expressed in dopaminergic neurons. However, upon feeding with 0.1% WGE,
274 we observed higher levels of GFP signal in both types of glia. Thus, overexpression of G2019S mutant
275 protein in dopaminergic neurons elicited reduced Nrf2 signaling activity, but WGE feeding restored or
276 further enhanced Nrf2 activities in these two glial subtypes.

277

278 **Nrf2 activation antagonizes BMP signaling in glia**

279 G2019S mutant protein in dopaminergic neurons has been shown previously to enhance the
280 expression of the proprotein convertase Furin 1 (Fur1) that processes the bone morphogenetic protein
281 (BMP) signaling molecule Glass bottom boat (Gbb) for maturation and release, leading to activation of
282 the BMP signaling pathway in glia (Maksoud et al., 2019). We confirmed that finding by removing one
283 copy of *Mad* that encodes the pathway's downstream effector to restore locomotion in *Ddc>G2019S* flies
284 (Figure 7-figure supplement 1). To address if WGE-induced Nrf2 activation could antagonize BMP
285 signaling activity in glia, first we assessed expression of the phosphorylated Mad (pMad) activated by
286 BMP signaling. In glia of *Ddc>G2019S* adult fly brains, pMad levels were higher than in *Ddc>Lrrk2*
287 brains and they could be suppressed by WGE treatment (Figure 7A and B). Similar to the previous report
288 (Maksoud et al., 2019), glial overexpression of Mad (*UAS-Mad*) or constitutively active type I receptor

289 Tkv (*UAS-tkv*^{Q253D}) was sufficient to impair locomotion, even without expressing G2019S mutant protein
290 in neurons. However, impaired locomotion was rescued in both cases by 0.1% WGE feeding (Figure 7C
291 and D). In addition, numbers of dopaminergic neurons in the PPL1 cluster were reduced upon glial
292 overexpression of *Mad* or *tkv*^{Q253D} and they were restored by 0.1% WGE treatment (Figure 7E to H).
293 Together, these analyses indicate that activation of BMP signaling in glia recapitulates the phenotypes
294 observed in flies overexpressing G2019S mutant protein in dopaminergic neurons and, furthermore, that
295 these effects can be suppressed by WGE treatment.

296 Next, we explored if WGE-induced Nrf2 activation antagonizes BMP signaling in glia. Glial Nrf2
297 overexpression in *Ddc-LexA>G2019S* flies (*Ddc-LexA>G2019S; repo>cncC-FL2*) partially rescued the
298 locomotory impairment caused by G2019S mutation (Figure 5B), and removing one copy of *Mad* (*Ddc-*
299 *LexA>G2019S, Mad*$^{+/-}$*; repo>cncC-FL2*) further enhanced this effect (Figure 8A). Indeed, this outcome
300 was equivalent to removing one copy of *Mad* but without Nrf2 overexpression (*Ddc-LexA>G2019S,*
301 *Mad*$^{+/-}$*; repo-GAL4*), suggesting that Nrf2 functions mainly to antagonize Mad activity (Figure 8A).
302 Consistently, Nrf2 overexpression in glia or WGE treatment suppressed the up-regulation of pMad levels
303 in glia caused by G2019S mutant protein overexpression in dopaminergic neurons (*Ddc-LexA>G2019S;*
304 *repo-GAL4*) (Figure 8B and C). Depletion of Nrf2 from glia (*Ddc-LexA>G2019S; repo>cnc-RNAi*), even
305 in the presence of WGE treatment, maintained high pMad levels in glia (Figure 8B and C). Thus,
306 modulation of Nrf2 activity, either by genetic manipulation or by WGE treatment, has an antagonistic
307 effect on pMad levels in glia.

308 We also addressed if *Mad* modulates expression of the Nrf2 target *ARE-GFP*. We observed
309 diminished GFP signal in PPL1-surrounding glia of *Ddc-LexA>G2019S* adult fly brains relative to the
310 *Ddc-LexA>Lrrk2* control. Heterozygosity of *Mad* in *Ddc-LexA>G2019S* flies (*Ddc-LexA>G2019S,*
311 *Mad*$^{+/-}$) restored the level of GFP signal, implying that Mad modulates targeted gene expression induced
312 by Nrf2 activity (Figure 8D and E).

313

314 **The effects of WGE treatment in a *LRRK2-G2019S* mouse model**

315 To further study the effect of WGE on G2019S mutation-induced neurodegeneration in a
316 mammalian system, we fed *LRRK2-G2019S* transgenic mice with WGE starting at the age of 8.5 months,
317 i.e., prior to onset of impairments in locomotion and dopaminergic neurons (Chou et al., 2014). We
318 quantified three locomotor activities from video-tracking paths of an open-field test, i.e., accumulative
319 moving distance, average velocity, and percentage of time moving (Figure 9A and B). At the age of 8.5
320 months, three groups—non-transgenic (nTg), transgenic *LRRK2-G2019S*, and WGE-fed transgenic
321 *LRRK2-G2019S* mice—presented comparable locomotor activities. At 9.5 months of age, the *LRRK2-*
322 *G2019S* mice displayed clearly impaired locomotion, which was statistically significant at the age of 11.5
323 months relative to nTg littermates (Figure 9B), consistent with a previous report (Chen et al., 2012).
324 Importantly, the *LRRK2-G2019S* mice fed with WGE showed improved locomotion throughout the 3-
325 month treatment period, an outcome that was statistically significant at 11.5 months (Figure 9 A and B).
326 WGE treatment also suppressed the centrophobism displayed by *LRRK2-G2019S* mice (Figure 9A). We
327 also analyzed the gait of these three groups of mice (Figure 9C). Similar to our findings from the open
328 field test, stride length of *LRRK2-G2019S* mice was significantly reduced at 11.5 months, but it was
329 restored to the level of nTg mice by WGE feeding (Figure 9C and D). Collectively, these analyses show
330 that WGE feeding is an effective means of restoring G2019S mutation-induced locomotory declines in
331 this mouse model of PD.

332 Since the nigral-striatal system contributes to locomotor function, we counted the number of TH-
333 positive dopaminergic neurons in the substantia nigra. In comparison to nTg littermates, the number of
334 dopaminergic neurons in 11.5-month-old *LRRK2-G2019S* mice was significantly reduced, but WGE
335 treatment for three months abrogated this loss of dopaminergic neurons (Figure 10A and B). In the
336 *Ddc>G2019S Drosophila* model, glia mediate the protective effects of WGE on dopaminergic neurons.
337 We found that activated microglia marked by ionized calcium-binding adapter molecule 1 (Iba-1) were
338 increased in the substantia nigra of *LRRK2-G2019S* mice, but this increase was suppressed by WGE
339 treatment (Figure 10C and D). We further analyzed levels of activated LRRK2 (pLRRK2) in lysates
340 isolated from the nigra-striatum. Levels of pLRRK2 normalized to LRRK2 signal were higher in *LRRK2-*

341 *G2019S* mice than in nTg littermates, but WGE treatment partially abrogated that outcome (Figure 10E
342 and F). Since G2019S mutation enhanced Mad signaling activation in the fly brain (Figure 8B and C), we
343 also tested this scenario in the mouse model. Immunoblots revealed that the ratio of phosphorylated
344 Smad2 to total Smad2 (pSmad2/Smad2) was significantly elevated in *LRRK2-G2019S* mice, but this
345 increase was suppressed by WGE treatment (Figure 10E and G). Moreover, although the level of
346 pSmad3/Smad3 was not significantly enhanced by G2019S mutant protein expression, it was suppressed
347 by WGE treatment (Figure 10E and G). Thus, WGE feeding suppresses G2019S mutation-induced
348 microglia activation and Smad signaling in the substantia nigra of the *LRRK2-G2019S* mouse model of
349 PD.

350 In summary, the potential mechanisms of WGE involved in the modulation of the neuron-glial
351 interaction are proposed (Figure 11). WGE regulates the hyperactivation of G2019S mutant protein in
352 dopaminergic neurons, and antagonizes the Mad signaling by activating the Nrf2 pathway in glia. Both
353 actions provide neuroprotection.

354

355 **Discussion**

356 Motor dysfunction in *Drosophila* neurodegeneration models has been frequently evaluated by means
357 of negative-geotaxis assay that measures the insect innate response. The assay begins with a sudden
358 external stimulation, which initially inhibits spontaneous locomotion but is followed by climbing
359 behavior. The entire response requires motor circuit coordination and muscle tone regulation, two
360 processes that progressively decline with age and that are impacted by neuropathological insults
361 (Grotewiel et al., 2005). In contrast, the open-arena walking assay allows free exploration without
362 disturbance, representing an assay for locomotor activities that can reveal deficits like bradykinesia (Chen
363 et al., 2014). Our G2019S flies exhibited reduced locomotor activity in both assays. Moreover, the
364 G2019S flies also exhibited centrophobism-like behavior in the open-arena (Figure 1D). Centrophobism
365 is indicative of emotional abnormalities, such as anxiety and depression, both of which are often
366 associated with PD (Kulisevsky et al., 2008), and was also displayed by the *LRRK2-G2019S* mice (Figure
367 9A). WGE treatment suppresses centrophobism in both fly and mouse PD models has important
368 implications for tackling major symptoms of PD and even non-PD-related depression, as reported for
369 rodent models (Lin et al., 2018; Y. E. Lin et al., 2016). Thus, WGE treatment exerts beneficial effects in
370 both of our PD models.

371 We found that the 0.1% dosage of WGE is optimal in suppressing age-dependent locomotion decline
372 in G2019S flies, with higher and lower doses being less effective (Figure 1A and Figure 1-figure
373 supplement 1B). Although an inverted U-shaped drug response is common, a plausible explanation for the
374 diminished effectiveness of higher doses is that WGE downregulates the day-time but not night-time
375 locomotor activity of flies (Jo et al., 2017). In mice, higher WGE doses have sleep-promoting effects by
376 activating adenosine A_1/A_2A receptors in the ventrolateral preoptic area (Zhang et al., 2012). Thus,
377 dosage level is critical to the beneficial effects of GE in both PD models.

378 Gastrodin and 4-HBA are considered the principal active components in GE (Zhan et al., 2016).
379 Although both compounds can cross the blood-brain barrier (Wu et al., 2017), the capability of gastrodin
380 to do so is relatively poor compared to aglyconic 4-HBA due to the glucose moiety (Lin et al., 2007).

381 Gastrodin is quickly metabolized to 4-HBA and undetermined metabolites in the brain (Lin et al., 2008),
382 perhaps explaining the lower effectiveness of gastrodin in G2019S flies. However, it is likely that the
383 combination of gastrodin with other components in GE might exert optimal beneficial effects.

384 Expression of G2019S mutant protein impacts different clusters of dopaminergic neurons in the fly
385 brain that are known for their connectivity and function. Activation of two specific mushroom body
386 (MB)-projection dopaminergic neurons in the PPL1 cluster inhibits climbing performance (Sun et al.,
387 2018). Mutations in the circadian gene *Clock* (*Clk*) cause PPL1 dopaminergic neuron degeneration,
388 accelerating impaired age-associated climbing ability (Vaccaro et al., 2017). Dopaminergic neurons in the
389 PPL2 cluster extend processes to the calyx of the MB, which has been linked to climbing activity (Sun et
390 al., 2018). In contrast, PPM3 neurons project to the central complex, activation of which enhances
391 locomotion (Kong et al., 2010). A significant reduction in dopaminergic neurons in the PPM1/2 cluster
392 was only found at week 4 when impaired locomotion of G2019S flies was prominent. In a PD fly model
393 involving *SNCA* overexpression and *aux* knockdown, dopaminergic neurons in the PPM1/2 cluster were
394 selectively degenerated and this phenotype was accompanied by impaired locomotion in relatively young
395 adult flies (Song et al., 2017). We postulate that the age-dependent impaired locomotion displayed by
396 G2019S flies could be caused by gradual and differential loss of dopaminergic neurons in these clusters,
397 thereby affecting different aspects of locomotion. However, further study is needed to test that hypothesis.

398 Expression of the G2019S mutant protein induces Lrrk2 auto- and hyper-phosphorylation, as well as
399 protein accumulation, together enhancing cellular Lrrk2 activity and causing aberrant downstream
400 signaling (Sheng et al., 2012). We have shown here that neuronal expression of Lrrk2-G2019S reduced
401 Akt phosphorylation (Figure 4A and B). Consistently, hyperactivated G2019S mutant protein impaired
402 interaction with and phosphorylation of Akt, resulting in compromised signaling and accelerated
403 neurodegeneration (Ohta et al., 2011; Panagiotakopoulou et al., 2020). However, WGE feeding restored
404 downstream Akt signaling by suppressing G2019S mutant protein hyperactivation. Rab10, one of the
405 best-characterized substrates for Lrrk2, mediates several of Lrrk2's cellular functions (Karayel et al.,
406 2020). In *Drosophila*, Rab10 and Lrrk2-G2019S synergistically affect the activity of dopaminergic

407 neurons, mediating deficits in movement (Fellgett et al., 2021; Petridi et al., 2020). We have shown that
408 WGE treatment downregulated levels of Lrrk2 accumulation and phosphorylated Rab10 (Figure 3F to H),
409 thus alleviating their synergistic toxicity. Several kinase inhibitors have been developed to block the
410 kinase activity of Lrrk2, including of both wild-type Lrrk2 and the G2019S mutant, which could affect
411 endogenous Lrrk2 activity (Sheng et al., 2012). Instead, WGE treatment modulates the phosphorylation
412 status and protein level of the G2019S mutant but not those of wild-type Lrrk2. The new hydrogen bond
413 created at the Ser^{2019} autophosphorylation site may provide a docking site for some chemicals in WGE,
414 representing a possible explanatory mechanism that warrants further study (Lang et al., 2015).

415 The antioxidation and detoxification factor Nrf2 is a target of Akt activation. Nrf2 phosphorylation and
416 HO-1 expression levels revealed that Nrf2 is inactivated in G2019S flies, but it was activated by WGE
417 treatment (Figure 4C and D). Intriguingly, our genetic data indicate that Nrf2 primarily functions in the
418 glia of G2019S flies, with Nrf2 depletion from glia eliminating the beneficial effects of WGE and glial
419 Nrf2 activation partially substituting for WGE feeding (Figure 5B). Cortical neurons express much lower
420 levels of Nrf2 than astrocytes owing to hypo-acetylation and transcriptional repression of the *Nrf2*
421 promoter (Bell et al., 2015). Moreover, neurons express greater amounts of Cullin 3, the scaffold
422 component of the E3 ubiquitin ligase that targets Nrf2 for proteasomal degradation (Jimenez-Blasco et al.,
423 2015). Both those mechanisms render neuronal Nrf2 inert to activation. Nrf2 activation in astrocytes
424 maintains neuronal integrity and function against oxidative insults in response to stress by supplying
425 antioxidants such as glutathione and HO-1 (Kraft et al., 2004; Vargas & Johnson, 2009). Previous study
426 showed that 4-HBA triggers glia to secrete HO-1 via the Nrf2 pathway, protecting neurons from hydrogen
427 peroxide in the primary culture (Luo et al., 2017). In PD models in which wild-type or mutant α-
428 synuclein is overexpressed, activation of neuronal Nrf2 (Barone et al., 2011; Skibinski et al., 2017) or
429 astrocytic Nrf2 (Gan et al., 2012) proved neuroprotective. By genetically manipulating the G2019S fly
430 model, we have shown that WGE-induced Nrf2 activation in glia but not in neurons protects
431 dopaminergic neurons from degeneration and ameliorates impaired locomotion.

432 Astrocyte-like and ensheathing glia are two major types of glia in the *Drosophila* nervous system,
433 surrounding and also extending long processes into neuropils of the brain. These astrocyte-like glia
434 exhibit a morphology and function similar to those of mammalian astrocytes, including reuptake of
435 neurotransmitters and phagocytosis of neuronal debris (Freeman, 2015; Tasdemir-Yilmaz & Freeman,
436 2014). Ensheathing glia of varying morphologies encase axonal tracts and neuropils, regulating neuronal
437 excitability and participating in phagocytosis and injury-induced inflammation (Doherty et al., 2009; Otto
438 et al., 2018). Thus, given their proximity to neurons and similar functions, it is not surprising that both
439 types of glia collectively mediate the protective effects of WGE.

440 Communication between neurons and glia maintains homeostasis, yet also confers the disease state
441 during neurodegeneration. In the *Drosophila* G2019S model, upregulation of the BMP ligand Gbb in
442 dopaminergic neurons activates Mad/Smad signaling in glia, which promotes neuronal degeneration via a
443 feedback mechanism (Maksoud et al., 2019). Surprisingly, although the number of dopaminergic neurons
444 in the fly brain is relatively small, the upregulated pMad signal spreads throughout the brain (Figure 7B),
445 suggesting that BMP can be disseminated over long distances. In PD patients, higher levels of TGF-β1
446 have been detected in the striatum and ventricular cerebrospinal fluid (Vawter et al., 1996). Thus,
447 members of the TGF-β1 superfamily such as TGF-β1 and BMP signaling molecules may represent
448 indicators of neuronal degeneration. Accordingly, disrupting the glia-to-neuron feedback mechanism may
449 sustain neuronal survival. In glia, we found that WGE treatment downregulated the pMad levels that had
450 been increased in the G2019S flies (Figure 7A and B). Nrf2 activation in glia also suppressed the
451 enhanced levels of pMad in G2019S flies (Figure 8B and C). Indeed, our genetic assays indicate that the
452 Nrf2 and Mad pathways interact in the glia of G2019S flies. Thus, WGE exerts its beneficial effects by
453 activating Nrf2 to antagonize the Mad activity that would otherwise contribute to the degeneration of
454 dopaminergic neurons. As a transcriptional activator, Nrf2 induces expression of the inhibitory
455 component Smad7 to form inactive Smad complexes (Song et al., 2019) and the phosphatase subunit
456 PPM1A to alter Smad2/3/4 phosphorylation and DNA binding (Lin et al., 2006). Given that these

457 components are conserved in *Drosophila*, Nrf2 may employ similar pathways to block Mad signaling in
458 glia.

459 That glial Nrf2 activation protects neurons is evidenced by our observations of enhanced HO-1
460 expression (Figure 4C) and increased numbers of dopaminergic neurons (Figure 5E and F). These results
461 support that the role of Nrf2 in glia is to induce expression of antioxidation building blocks, such as
462 phase-II detoxification enzymes, and to enhance inflammatory processes (Hirrlinger & Dringen, 2010;
463 Rojo et al., 2010). In a model of fibrosis, TGF-β/Smad2/3 suppressed expression of the *ARE*-luciferase
464 reporter and gluthathion (Ryoo et al., 2014). Moreover, Nrf2 knockdown was shown to reduce expression
465 of the antioxidative enzyme NAD(P)H quinone dehydrogenase 1 (NQO1), thereby elevating cellular
466 oxidative stress and upregulating TGF-β/Smad targeted gene expression (Prestigiacomo & Suter-Dick,
467 2018). Hence, we propose that WGE promotes Nrf2 activation to antagonize the Smad signaling in glia
468 that is induced by dopaminergic neuron-secreted BMP/Gbb signal during degeneration.

469 By employing a *LRRK2-G2019S* mouse model, we have also demonstrated that WGE rescues their
470 locomotor coordination, suppresses their centrophobism, and recovers their numbers of dopaminergic
471 neurons and hyperactivated microglia (Figure 9, and Figure 10A to D). Significantly, we found that
472 activity of the TGF-β/Smad2/3 pathway was elevated in nigrostriatal brain lysates, and this activity was
473 also suppressed by WGE treatment (Figure 10E and G). Collectively, these results from fly and mouse PD
474 models indicate that the effectiveness of WGE is likely mediated through conserved Nrf2/Mad pathways
475 (Figure 11). Our findings contribute to our mechanistic understanding of PD and provide potential
476 therapeutic strategies that incorporate the traditional herbal medicine GE.

477

478 **Materials and Methods**

479 ***Drosophila* stocks and maintenance**

480 All fly stocks were maintained on standard cornmeal-based food medium at 25°C. *Drosophila* stocks
481 sourced from the Bloomington *Drosophila* Stock Center (Indiana University, Bloomington, USA) were:
482 *UAS-mCD8-GFP* (#5137), *elav-GAL4* (#8760), *repo-GAL4* (#7215), *Ddc-LexA* (#54218), *UAS-cncTRiP*
483 (#25984), *Tub-GAL80*^{ts} (#7108), *alrm-GAL4* (#67032), *R56F03-GAL4* (#39157), *UAS-tkv*^{Q253D} (#36536),
484 and *Mad*^{K00237} (#10474). *NP2222-GAL4* (#112830) was from the *Drosophila* Genomics Resource Center
485 and *NP6293-GAL4* (#105188) was from the Kyoto Stock Center. Other stocks include *UAS-Flag-LRRK2-*
486 *WT* (Lin et al., 2010), *UAS-Flag-LRRK2-G2019S* (Lin et al., 2010), *Ddc-GAL4* (Sang et al., 2007), *ARE-*
487 *GFP* (Sykiotis & Bohmann, 2008), *GstD-GFP* (Sykiotis & Bohmann, 2008), *UAS-cncC-FL2* (Sykiotis &
488 Bohmann, 2008), *moody-GAL4* (Bainton et al., 2005), and *UAS-Mad* (Takaesu et al., 2006). The two
489 *LexAop* fly lines—*LexAop-LRRK2-WT* and *LexAop-LRRK2-G2019S*—were generated in this study. In
490 brief, the cDNAs for *LRRK2-WT* and *LRRK2-G2019S* were isolated from plasmids (Invitrogen, California,
491 USA) for subcloning into *LexAop* plasmids (Addgene, Massachusetts, USA), which were for
492 microinjection (Fly facility, University of Cambridge, UK). The transgenes were site landed at an attP site
493 on the 2nd chromosome (25C6). For temperature-shift assay of *GAL80*^{ts} flies, parental flies were
494 maintained at 19°C and allowed to mate, before collecting the F1 adults and shifting them to 29°C to
495 inactivate GAL80.

496

497 **Preparation of WGE and related chemical compounds**

498 Authentication of GE and preparation of WGE were as described previously (Lin et al., 2018; Y. E.
499 Lin et al., 2016). WGE (KO DA Pharmaceutical Co. Ltd., Taoyuan, Taiwan), gastrodin (Wuhan YC Fine
500 Chemical Co., Wuhan, China), and 4-HBA (Sigma-Aldrich, Darmstadt, Germany) were added to freshly-
501 prepared cornmeal-based fly food at indicated final concentrations (w/w). For experiments, one- to three-
502 day-old post-eclosion flies were collected and transferred to fresh food medium twice per week.

503

504 **Fly locomotion assay**

505 A negative geotaxis climbing assay was performed to assess locomotor activity, and it was
506 conducted according to a previous study with minor modification (Madabattula et al., 2015). Cohorts of
507 35 flies from each genotype were assayed weekly for six consecutive weeks. Success rates were
508 calculated as the percentage of flies that could climb above the 8-cm mark of a 20-cm cylinder within 10
509 s.

510 The free-walking assay protocol was conducted based on a previous report with minor modification
511 (Chen et al., 2014). Cohorts of eight flies were habituated on a 10-cm agar-filled dish for 30 min. The
512 dishes were gently tapped to encourage the flies to walk, which was video-taped for 5 min. Movement
513 tracks were processed in ImageJ and quantified using the Caltech multiple fly tracker (Ctrax).

514

515 **Immunostaining and immunoblotting of adult fly brains**

516 The protocol for immunostaining whole-mount adult brains was essentially as described previously
517 (Lin et al., 2010; Maksoud et al., 2019). Adult fly brains for each genotype were dissected at the indicated
518 time-points for immunostaining with the following primary antibodies: mouse anti-TH (Immunostar,
519 22941, 1:1000); mouse anti-repo (Hybridoma Bank DSHB, 8D12, 1:500); chicken anti-GFP (Abcam,
520 ab13970, 1:10000); and rabbit anti-phospho-Smad3 (Ser423/425) (Abcam, ab52903, 1:250) (Smith et al.,
521 2012). Fluorophore-conjugated secondary antibodies were: FITC-conjugated goat anti-mouse IgG
522 (Jackson Lab, AB_2338589, 1:500); Alexa Fluor 488-conjugated goat anti-mouse IgG (Invitrogen,
523 A28175, 1:500); Cy3-conjugated goat anti-mouse IgG (Jackson Lab, AB_2338680, 1:500); Alexa Fluor
524 488-conjugated goat anti-rabbit IgG (Invitrogen, A27034, 1:500); and Cy5-conjugated goat anti-rat IgG
525 (Invitrogen, A10525, 1:500). Phalloidin-TRITC (Sigma, P1951, 1:5000) that binds F-actin was also used
526 for counterstaining. Immunofluorescence signals were acquired under confocal microscopy (ZEISS LSM
527 710, Germany).

528 Adult brain extracts were prepared according to a previously described protocol (Lin et al., 2010). In
529 brief, ~80 fly heads for each genotype were isolated for extract preparation. Equivalent amounts of

530 samples (30 μg/20 μL/well) were resolved by SDS-PAGE for immunoblotting. The following primary
531 antibodies were used: rabbit anti-human LRRK2 (Abcam, ab133474, 1:1000); rabbit anti-phospho-
532 LRRK2 (Ser^{1292}) (Abcam, ab203181, 1:500); rabbit anti-Akt (Cell Signaling, #4691, 1:1000); rabbit anti-
533 *Drosophila* phospho-Akt Ser^{505} (Cell Signaling, #4054, 1:500); rabbit anti-Nrf2 (Thermo, 710574,
534 1:1000); rabbit anti-phospho-Nrf2 (Ser^{40}) (Thermo Fisher Scientific, PA5-67520, 1:1000); mouse anti-
535 HO-1-1 (Thermo Fisher Scientific, MA1-112, 1:1000); rabbit anti-GAPDH (GeneTex, GTX100118,
536 1:5000); and rabbit anti-alpha tubulin (Cell Signaling, #2144, 1:10000), followed by blotting with
537 secondary antibodies peroxidase-conjugated goat anti-rabbit IgG (Jackson Lab, AB_2307391, 1:7500)
538 and peroxidase-conjugated goat anti-mouse IgG (Jackson Lab, AB_10015289, 1:7500).
539

540 ***ARE-GFP* reporter assay**

541 The antioxidant response element (*ARE)-GFP* reporter assay was a modification of the protocol
542 from a previous study (Sykiotis & Bohmann, 2008). One-day old virgin female flies (homozygous for
543 *ARE-GFP*) were mated for one day, and then fed with regular food or food containing 0.1% WGE for two
544 more days before imaging for GFP signals. To immunostain the *ARE-GFP* reporter signal in brain,
545 feeding of 0.1% WGE was extended to 5 days. To quantify *ARE-GFP* in adult fly brain, the 0.5-μm
546 confocal images were processed in ImageJ. Mean *ARE-GFP* fluorescence intensities of *mCherry*-labeled
547 glial cells in the PPL1 neuronal cluster were quantified by manually outlining the labeled area to first
548 measure mean GFP signal and then normalizing it to mCherry signal (GFP/mCherry).
549

550 **Animal care and treatments**

551 Transgenic *LRRK2-G2019S* mice were purchased from Jackson Laboratory (JAX stock #009609,
552 Bar Harbor, ME, USA) and they were maintained at the animal center of the National Taiwan University
553 Hospital (NTUH). Non-transgenic (nTg) and heterozygous transgenic *LRRK2-G2019S* mice were
554 obtained by crossing heterozygous *LRRK2-G2019S* mice with wild-type FVB/NJ mice. Mice at 8.5

555 months-old were assigned to one of three groups (5 to 6 mice per group): nTg, *LRRK2-G2019S,* and
556 *LRRK2-G2019S* fed with WGE (0.5 g/kg body weight per day) (Lin et al., 2018) for three months.
557

558 **Behavioral assays**

559 We employed two behavioral tests to assay mouse motor function, i.e., an open field assay to assess
560 spontaneous locomotor activity and CatWalk XT gait analysis to assay coordination. Behavioral
561 experiments were conducted blind to genotype, as described previously (Lin et al., 2020).
562

563 **Immunohistochemical staining**

564 After three months of WGE treatment, mice were sacrificed at the age of 11.5 months. The
565 substantia nigra and striatum were dissected out. The substantia nigra was subjected to immunostaining,
566 as described previously (Lin et al., 2020). Anti-tyrosine hydroxylase (TH) (Millipore, AB152, 1:200) and
567 anti-ionized calcium-binding adapter molecule 1 (Iba-1) (GeneTex, GTX100042, 1:200) were used as
568 primary antibodies for 24 h at 4°C. Secondary antibodies were DyLight 488 goat anti-rabbit 1:300 and
569 DyLight 546 goat anti-rabbit at 1:200 (25°C for 1 h). Mounting medium with DAPI (GeneTex,
570 GTX30920) was used as a counterstain.
571

572 **Immunoblotting**

573 Frozen nigrostriatal brain tissues were homogenized and mixed with lysis buffer to determine
574 protein content and for immunoblotting, as described previously (Lin et al., 2020). The membrane was
575 incubated overnight at 4°C with the following primary antibodies: anti-LRRK2 (Abcam, ab133474,
576 1:5000); anti-phospho-LRRK2 (Ser^{1292}, Abcam, ab203181, 1:1000); anti-Smad2 (Cell Signaling, 5339T,
577 1:1000); anti-phospho-Smad2 (Ser465/467, Cell Signaling, 3108T, 1:1000); anti-Smad3 (Cell Signaling,
578 9523T, 1:1000); anti-phospho-Smad3 (Ser423/425, Abcam, ab52903, 1:1000); and anti-beta actin
579 (Sigma-Aldrich, A5441, 1:5000). After washing, peroxidase-conjugated goat anti-rabbit IgG (GeneTex,

580 GTX213110-01, 1:5000) or peroxidase-conjugated goat anti-mouse IgG (GeneTex, GTX213111-01,
581 1:5000) were used as secondary antibodies.
582
583 **Statistical Analysis**
584 All statistical analyses were carried out in GraphPad PRISM 6 (La Jolla, CA, USA). Data are
585 presented as mean ± standard error (SEM). Statistical analysis was performed using either student *t*-test or
586 one-way analysis of variance (ANOVA) followed by Tukey's multiple comparison test. *P* values less than
587 0.05 ($p < 0.05$) were considered indicative of significance. For exact n numbers, *p* values, F values, t-
588 values, and degrees of freedom of each statistical test, please see the statistical information in the
589 Additional file-Supporting file 2.
590

591 **Acknowledgements**

592 We thank D. Bohmann (URMC), U. Heberlein (HHMI), S. J. Newfeld (ASU), T.-K. Sang (NTHU),
593 Bloomington Stock Center, *Drosophila* Genomics Resource Center, Kyoto Stock Center and Taiwan Fly
594 Core for providing fly stocks. We thank KO DA Pharmaceutical Co. Ltd. (Taoyuan, Taiwan) and Wuhan
595 YC Fine Chemical Co. (Wuhan, China) for providing WGE and gastrodin, respectively.

596

597 **Additional information**

598 **Ethics approval**

599 All animal procedures were approved by the local ethics committee and the Institutional Animal
600 Care and Use Committee (IACUC) of the National Taiwan University (IACUC approval no. 20180103).

601

602 **Data availability**

603 All data generated or analyzed during this study are included in the manuscript and supporting files.

604

605 **Competing interests**

606 The authors declare that they have no competing interests.

607

608 **Funding**

609 This work was supported by grants from the Taiwan Ministry of Science and Technology (MOST-
610 108-2311-B-001-039-MY3) to C.-T. C. S.P. and C.J.H.E. were supported by Parkinson's Disease Society
611 of the United Kingdom (Parkinson's UK), grant H1201.

612

613 **Authors' contributions**

614 Y.-E.L., C.-H.L., L.-Y.S., and C.-T.C. designed the research. Y.-E.L., E.-P.H., and Y.-C.K. performed
615 the experiments. S.P. and C.J.H.E. contributed new reagents. Y.-E.L., C.-H.L., E.-P.H., and Y.-C.K.

616 analyzed the data. Y.-E.L., C.-H.L., L.-Y.S. and C.-T.C. drafted and revised the manuscript. All authors

617 have read and approved the final manuscript.

618

619 **Additional files**

620 **Supporting file 1**

621 Figure supplements.pdf

622 **Figure 1-figure supplement 1.** Climbing activity assay of *Ddc>mCD8-GFP* and *Ddc>Lrrk2* flies.

623 **Figure 2-figure supplement 1.** WGE treatment prevents dopaminergic neuron loss in *Ddc>G2019S* flies.

624 **Figure 3-figure supplement 1.** WGE specifically modulates Lrrk2 accumulation and hyperactivation in

625 *elav>G2019S* but not *elav>Lrrk2* flies.

626 **Figure 5-figure supplement 1.** WGE rescues the locomotion defect displayed by *Ddc-LexA>G2019S*

627 flies.

628 **Figure 6-figure supplement 1.** Lrrk2 and pLrrk2 levels are maintained upon glial Nrf2 overexpression.

629 **Figure 7-figure supplement 1.** *Mad* heterozygosity rescues the impaired locomotion of *Ddc>G2019S*

630 flies.

631

632 **Supporting file 2**

633 Source data 1-Statistical Information.xlsx

634 The file includes all data and the statistical analyses in this article and its supplementary information.

635

636 **Supporting file 3**

637 Source data 2-Data-WB.pdf

638 The file includes the uncropped images of the western blotting in this article.

639

640 **References**

641 Angeles, D. C., Gan, B. H., Onstead, L., Zhao, Y., Lim, K. L., Dachsel, J., Melrose, H., Farrer, M.,
642 Wszolek, Z. K., Dickson, D. W., & Tan, E. K. (2011). Mutations in LRRK2 increase
643 phosphorylation of peroxiredoxin 3 exacerbating oxidative stress-induced neuronal death. *Hum*
644 *Mutat*, *32*(12), 1390-1397. https://doi.org/10.1002/humu.21582

645 Bainton, R. J., Tsai, L. T., Schwabe, T., DeSalvo, M., Gaul, U., & Heberlein, U. (2005). *moody* encodes
646 two GPCRs that regulate cocaine behaviors and blood-brain barrier permeability in *Drosophila*.
647 *Cell*, *123*(1), 145-156. https://doi.org/10.1016/j.cell.2005.07.029

648 Barone, M. C., Sykiotis, G. P., & Bohmann, D. (2011). Genetic activation of Nrf2 signaling is sufficient
649 to ameliorate neurodegenerative phenotypes in a *Drosophila* model of Parkinson's disease. *Dis*
650 *Model Mech*, *4*(5), 701-707. https://doi.org/10.1242/dmm.007575

651 Bell, K. F., Al-Mubarak, B., Martel, M. A., McKay, S., Wheelan, N., Hasel, P., Markus, N. M., Baxter, P.,
652 Deighton, R. F., Serio, A., Bilican, B., Chowdhry, S., Meakin, P. J., Ashford, M. L., Wyllie, D. J.,
653 Scannevin, R. H., Chandran, S., Hayes, J. D., & Hardingham, G. E. (2015). Neuronal
654 development is promoted by weakened intrinsic antioxidant defences due to epigenetic repression
655 of Nrf2. *Nat Commun*, *6*, 7066. https://doi.org/10.1038/ncomms8066

656 Chatterjee, N., & Bohmann, D. (2012). A versatile PhiC31 based reporter system for measuring AP-1 and
657 Nrf2 signaling in *Drosophila* and in tissue culture. *PLoS One*, *7*(4), e34063.
658 https://doi.org/10.1371/journal.pone.0034063

659 Chen, A. Y., Wilburn, P., Hao, X., & Tully, T. (2014). Walking deficits and centrophobism in an alpha-
660 synuclein fly model of Parkinson's disease. *Genes Brain Behav*, *13*(8), 812-820.
661 https://doi.org/10.1111/gbb.12172

662 Chen, C. Y., Weng, Y. H., Chien, K. Y., Lin, K. J., Yeh, T. H., Cheng, Y. P., Lu, C. S., & Wang, H. L.
663 (2012). (G2019S) LRRK2 activates MKK4-JNK pathway and causes degeneration of SN
664 dopaminergic neurons in a transgenic mouse model of PD. *Cell Death Differ*, *19*(10), 1623-1633.
665 https://doi.org/10.1038/cdd.2012.42

666 Chen, L., & Feany, M. B. (2005). Alpha-synuclein phosphorylation controls neurotoxicity and inclusion
667 formation in a *Drosophila* model of Parkinson disease. *Nat Neurosci*, *8*(5), 657-663.
668 https://doi.org/10.1038/nn1443

669 Chen, P. J., & Sheen, L. Y. (2011). *Gastrodiae Rhizoma* (tian ma): a review of biological activity and
670 antidepressant mechanisms. *J Tradit Complement Med*, *1*(1), 31-40.
671 https://www.ncbi.nlm.nih.gov/pubmed/24716103

672 Chen, W. C., Lai, Y. S., Lin, S. H., Lu, K. H., Lin, Y. E., Panyod, S., Ho, C. T., & Sheen, L. Y. (2016).
673 Anti-depressant effects of *Gastrodia elata* Blume and its compounds gastrodin and 4-

674 hydroxybenzyl alcohol, via the monoaminergic system and neuronal cytoskeletal remodeling. *J*
675 *Ethnopharmacol*, *182*, 190-199. https://doi.org/10.1016/j.jep.2016.02.001
676 Chou, J. S., Chen, C. Y., Chen, Y. L., Weng, Y. H., Yeh, T. H., Lu, C. S., Chang, Y. M., & Wang, H. L.
677 (2014). (G2019S) LRRK2 causes early-phase dysfunction of SNpc dopaminergic neurons and
678 impairment of corticostriatal long-term depression in the PD transgenic mouse. *Neurobiol Dis*, *68*,
679 190-199. https://doi.org/10.1016/j.nbd.2014.04.021
680 Clark, I. E., Dodson, M. W., Jiang, C., Cao, J. H., Huh, J. R., Seol, J. H., Yoo, S. J., Hay, B. A., & Guo,
681 M. (2006). *Drosophila pink1* is required for mitochondrial function and interacts genetically with
682 *parkin*. *Nature*, *441*(7097), 1162-1166. https://doi.org/10.1038/nature04779
683 Doherty, J., Logan, M. A., Tasdemir, O. E., & Freeman, M. R. (2009). Ensheathing glia function as
684 phagocytes in the adult *Drosophil*a brain. *J Neurosci*, *29*(15), 4768-4781.
685 https://doi.org/10.1523/JNEUROSCI.5951-08.2009
686 Fellgett, A., Middleton, C. A., Munns, J., Ugbode, C., Jaciuch, D., Wilson, L., Chawla, S., & Elliott, C. J.
687 H. (2021). Multiple pathways of LRRK2-G2019S/Rab10 interaction in dopaminergic neurons. *J*
688 *Parkinsons Dis*. https://doi.org/10.3233/JPD-202421
689 Freeman, M. R. (2015). *Drosophila* central nervous system glia. *Cold Spring Harb Perspect Biol*, *7*(11).
690 https://doi.org/10.1101/cshperspect.a020552
691 Gan, L., Vargas, M. R., Johnson, D. A., & Johnson, J. A. (2012). Astrocyte-specific overexpression of
692 Nrf2 delays motor pathology and synuclein aggregation throughout the CNS in the alpha-
693 synuclein mutant (A53T) mouse model. *J Neurosci*, *32*(49), 17775-17787.
694 https://doi.org/10.1523/JNEUROSCI.3049-12.2012
695 Grotewiel, M. S., Martin, I., Bhandari, P., & Cook-Wiens, E. (2005). Functional senescence in
696 *Drosophila* melanogaster. *Ageing Res Rev*, *4*(3), 372-397.
697 https://doi.org/10.1016/j.arr.2005.04.001
698 Henry, A. G., Aghamohammadzadeh, S., Samaroo, H., Chen, Y., Mou, K., Needle, E., & Hirst, W. D.
699 (2015). Pathogenic LRRK2 mutations, through increased kinase activity, produce enlarged
700 lysosomes with reduced degradative capacity and increase ATP13A2 expression. *Hum Mol Genet*,
701 *24*(21), 6013-6028. https://doi.org/10.1093/hmg/ddv314
702 Hirrlinger, J., & Dringen, R. (2010). The cytosolic redox state of astrocytes: Maintenance, regulation and
703 functional implications for metabolite trafficking. *Brain Res Rev*, *63*(1-2), 177-188.
704 https://doi.org/10.1016/j.brainresrev.2009.10.003
705 Houlden, H., & Singleton, A. B. (2012). The genetics and neuropathology of Parkinson's disease. *Acta*
706 *Neuropathol*, *124*(3), 325-338. https://doi.org/10.1007/s00401-012-1013-5

707 Jang, J. H., Son, Y., Kang, S. S., Bae, C. S., Kim, J. C., Kim, S. H., Shin, T., & Moon, C. (2015).
708 Neuropharmacological potential of *Gastrodia elata* Blume and its components. *Evid Based*
709 *Complement Alternat Med*, *2015*, 309261. https://doi.org/10.1155/2015/309261
710 Jiang, G., Hu, Y., Liu, L., Cai, J., Peng, C., & Li, Q. (2014). Gastrodin protects against MPP(+)-induced
711 oxidative stress by up regulates heme oxygenase-1 expression through p38 MAPK/Nrf2 pathway
712 in human dopaminergic cells. *Neurochem Int*, *75*, 79-88.
713 https://doi.org/10.1016/j.neuint.2014.06.003
714 Jimenez-Blasco, D., Santofimia-Castano, P., Gonzalez, A., Almeida, A., & Bolanos, J. P. (2015).
715 Astrocyte NMDA receptors' activity sustains neuronal survival through a Cdk5-Nrf2 pathway.
716 *Cell Death Differ*, *22*(11), 1877-1889. https://doi.org/10.1038/cdd.2015.49
717 Jo, K., Jeon, S., Ahn, C. W., Han, S. H., & Suh, H. J. (2017). Changes in *Drosophila* melanogaster sleep-
718 wake behavior due to lotus (*Nelumbo nucifera*) seed and Hwang Jeong (*Polygonatum sibiricum*)
719 extracts. *Prev Nutr Food Sci*, *22*(4), 293-299. https://doi.org/10.3746/pnf.2017.22.4.293
720 Jucaite, A., Svenningsson, P., Rinne, J. O., Cselenyi, Z., Varnas, K., Johnstrom, P., Amini, N.,
721 Kirjavainen, A., Helin, S., Minkwitz, M., Kugler, A. R., Posener, J. A., Budd, S., Halldin, C.,
722 Varrone, A., & Farde, L. (2015). Effect of the myeloperoxidase inhibitor AZD3241 on microglia:
723 a PET study in Parkinson's disease. *Brain*, *138*(Pt 9), 2687-2700.
724 https://doi.org/10.1093/brain/awv184
725 Kam, T. I., Hinkle, J. T., Dawson, T. M., & Dawson, V. L. (2020). Microglia and astrocyte dysfunction in
726 Parkinson's disease. *Neurobiol Dis*, *144*, 105028. https://doi.org/10.1016/j.nbd.2020.105028
727 Karayel, O., Tonelli, F., Virreira Winter, S., Geyer, P. E., Fan, Y., Sammler, E. M., Alessi, D. R., Steger,
728 M., & Mann, M. (2020). Accurate MS-based Rab10 phosphorylation stoichiometry determination
729 as readout for LRRK2 Activity in Parkinson's disease. *Mol Cell Proteomics*, *19*(9), 1546-1560.
730 https://doi.org/10.1074/mcp.RA120.002055
731 Kim, T. H., Cho, K. H., Jung, W. S., & Lee, M. S. (2012). Herbal medicines for Parkinson's disease: a
732 systematic review of randomized controlled trials. *PLoS One*, *7*(5), e35695.
733 https://doi.org/10.1371/journal.pone.0035695
734 Kong, E. C., Woo, K., Li, H., Lebestky, T., Mayer, N., Sniffen, M. R., Heberlein, U., Bainton, R. J.,
735 Hirsh, J., & Wolf, F. W. (2010). A pair of dopamine neurons target the D1-like dopamine receptor
736 DopR in the central complex to promote ethanol-stimulated locomotion in *Drosophila*. *PLoS One*,
737 *5*(4), e9954. https://doi.org/10.1371/journal.pone.0009954
738 Kraft, A. D., Johnson, D. A., & Johnson, J. A. (2004). Nuclear factor E2-related factor 2-dependent
739 antioxidant response element activation by tert-butylhydroquinone and sulforaphane occurring
740 preferentially in astrocytes conditions neurons against oxidative insult. *J Neurosci*, *24*(5), 1101-
741 1112. https://doi.org/10.1523/JNEUROSCI.3817-03.2004

742 Kulisevsky, J., Pagonabarraga, J., Pascual-Sedano, B., Garcia-Sanchez, C., Gironell, A., & Trapecio
743 Group, S. (2008). Prevalence and correlates of neuropsychiatric symptoms in Parkinson's disease
744 without dementia. *Mov Disord*, *23*(13), 1889-1896. https://doi.org/10.1002/mds.22246
745 Kumar, H., Kim, I. S., More, S. V., Kim, B. W., Bahk, Y. Y., & Choi, D. K. (2013). Gastrodin protects
746 apoptotic dopaminergic neurons in a toxin-induced Parkinson's disease model. *Evid Based*
747 *Complement Alternat Med*, *2013*, 514095. https://doi.org/10.1155/2013/514095
748 Lang, C. A., Ray, S. S., Liu, M., Singh, A. K., & Cuny, G. D. (2015). Discovery of LRRK2 inhibitors
749 using sequential in silico joint pharmacophore space (JPS) and ensemble docking. *Bioorg Med*
750 *Chem Lett*, *25*(13), 2713-2719. https://doi.org/10.1016/j.bmcl.2015.04.027
751 Li, X., Zhang, Y., Wang, Y., Xu, J., Xin, P., Meng, Y., Wang, Q., & Kuang, H. (2017). The mechanisms
752 of Traditional Chinese Medicine underlying the prevention and treatment of Parkinson's disease.
753 *Front Pharmacol*, *8*, 634. https://doi.org/10.3389/fphar.2017.00634
754 Lin, C. H., Lin, H. I., Chen, M. L., Lai, T. T., Cao, L. P., Farrer, M. J., Wu, R. M., & Chien, C. T. (2016).
755 Lovastatin protects neurite degeneration in LRRK2-G2019S parkinsonism through activating the
756 Akt/Nrf pathway and inhibiting GSK3beta activity. *Hum Mol Genet*, *25*(10), 1965-1978.
757 https://doi.org/10.1093/hmg/ddw068
758 Lin, C. H., Tsai, P. I., Lin, H. Y., Hattori, N., Funayama, M., Jeon, B., Sato, K., Abe, K., Mukai, Y.,
759 Takahashi, Y., Li, Y., Nishioka, K., Yoshino, H., Daida, K., Chen, M. L., Cheng, J., Huang, C. Y.,
760 Tzeng, S. R., Wu, Y. S., Lai, H. J., Tsai, H. H., Yen, R. F., Lee, N. C., Lo, W. C., Hung, Y. C.,
761 Chan, C. C., Ke, Y. C., Chao, C. C., Hsieh, S. T., Farrer, M., & Wu, R. M. (2020). Mitochondrial
762 UQCRC1 mutations cause autosomal dominant parkinsonism with polyneuropathy. *Brain*,
763 *143*(11), 3352-3373. https://doi.org/10.1093/brain/awaa279
764 Lin, C. H., Tsai, P. I., Wu, R. M., & Chien, C. T. (2010). LRRK2 G2019S mutation induces dendrite
765 degeneration through mislocalization and phosphorylation of tau by recruiting autoactivated
766 GSK3ss. *J Neurosci*, *30*(39), 13138-13149. https://doi.org/10.1523/JNEUROSCI.1737-10.2010
767 Lin, L. C., Chen, Y. F., Lee, W. C., Wu, Y. T., & Tsai, T. H. (2008). Pharmacokinetics of gastrodin and
768 its metabolite p-hydroxybenzyl alcohol in rat blood, brain and bile by microdialysis coupled to
769 LC-MS/MS. *J Pharm Biomed Anal*, *48*(3), 909-917. https://doi.org/10.1016/j.jpba.2008.07.013
770 Lin, L. C., Chen, Y. F., Tsai, T. R., & Tsai, T. H. (2007). Analysis of brain distribution and biliary
771 excretion of a nutrient supplement, gastrodin, in rat. *Anal Chim Acta*, *590*(2), 173-179.
772 https://doi.org/10.1016/j.aca.2007.03.035
773 Lin, L. F., Doherty, D. H., Lile, J. D., Bektesh, S., & Collins, F. (1993). GDNF: a glial cell line-derived
774 neurotrophic factor for midbrain dopaminergic neurons. *Science*, *260*(5111), 1130-1132.
775 https://doi.org/10.1126/science.8493557

776 Lin, X., Duan, X., Liang, Y. Y., Su, Y., Wrighton, K. H., Long, J., Hu, M., Davis, C. M., Wang, J.,
777 Brunicardi, F. C., Shi, Y., Chen, Y. G., Meng, A., & Feng, X. H. (2006). PPM1A functions as a
778 Smad phosphatase to terminate TGFbeta signaling. *Cell*, *125*(5), 915-928.
779 https://doi.org/10.1016/j.cell.2006.03.044
780 Lin, Y. E., Chou, S. T., Lin, S. H., Lu, K. H., Panyod, S., Lai, Y. S., Ho, C. T., & Sheen, L. Y. (2018).
781 Antidepressant-like effects of water extract of *Gastrodia elata* Blume on neurotrophic regulation
782 in a chronic social defeat stress model. *J Ethnopharmacol*, *215*, 132-139.
783 https://doi.org/10.1016/j.jep.2017.12.044
784 Lin, Y. E., Lin, S. H., Chen, W. C., Ho, C. T., Lai, Y. S., Panyod, S., & Sheen, L. Y. (2016).
785 Antidepressant-like effects of water extract of *Gastrodia elata* Blume in rats exposed to
786 unpredictable chronic mild stress via modulation of monoamine regulatory pathways. *J*
787 *Ethnopharmacol*, *187*, 57-65. https://doi.org/10.1016/j.jep.2016.04.032
788 Liu, Z., Wang, X., Yu, Y., Li, X., Wang, T., Jiang, H., Ren, Q., Jiao, Y., Sawa, A., Moran, T., Ross, C. A.,
789 Montell, C., & Smith, W. W. (2008). A *Drosophila* model for LRRK2-linked parkinsonism. *Proc*
790 *Natl Acad Sci U S A*, *105*(7), 2693-2698. https://doi.org/10.1073/pnas.0708452105
791 Luo, L., Kim, S. W., Lee, H. K., Kim, I. D., Lee, H., & Lee, J. K. (2017). Anti-oxidative effects of 4-
792 hydroxybenzyl alcohol in astrocytes confer protective effects in autocrine and paracrine manners.
793 *PLoS One*, *12*(5), e0177322. https://doi.org/10.1371/journal.pone.0177322
794 Madabattula, S. T., Strautman, J. C., Bysice, A. M., O'Sullivan, J. A., Androschuk, A., Rosenfelt, C.,
795 Doucet, K., Rouleau, G., & Bolduc, F. (2015). Quantitative analysis of climbing defects in a
796 *Drosophila* model of neurodegenerative disorders. *J Vis Exp*(100), e52741.
797 https://doi.org/10.3791/52741
798 Maksoud, E., Liao, E. H., & Haghighi, A. P. (2019). A neuron-glial trans-signaling cascade mediates
799 LRRK2-induced neurodegeneration. *Cell Rep*, *26*(7), 1774-1786 e1774.
800 https://doi.org/10.1016/j.celrep.2019.01.077
801 Mao, Z., & Davis, R. L. (2009). Eight different types of dopaminergic neurons innervate the *Drosophila*
802 mushroom body neuropil: anatomical and physiological heterogeneity. *Front Neural Circuits*, *3*, 5.
803 https://doi.org/10.3389/neuro.04.005.2009
804 Martin, I., Kim, J. W., Dawson, V. L., & Dawson, T. M. (2014). LRRK2 pathobiology in Parkinson's
805 disease. *J Neurochem*, *131*(5), 554-565. https://doi.org/10.1111/jnc.12949
806 Miklossy, J., Arai, T., Guo, J. P., Klegeris, A., Yu, S., McGeer, E. G., & McGeer, P. L. (2006). LRRK2
807 expression in normal and pathologic human brain and in human cell lines. *J Neuropathol Exp*
808 *Neurol*, *65*(10), 953-963. https://doi.org/10.1097/01.jnen.0000235121.98052.54

809 Moehle, M. S., Webber, P. J., Tse, T., Sukar, N., Standaert, D. G., DeSilva, T. M., Cowell, R. M., & West,
810 A. B. (2012). LRRK2 inhibition attenuates microglial inflammatory responses. *J Neurosci*, *32*(5),
811 1602-1611. https://doi.org/10.1523/JNEUROSCI.5601-11.2012
812 Nguyen, H. N., Byers, B., Cord, B., Shcheglovitov, A., Byrne, J., Gujar, P., Kee, K., Schule, B.,
813 Dolmetsch, R. E., Langston, W., Palmer, T. D., & Pera, R. R. (2011). LRRK2 mutant iPSC-
814 derived DA neurons demonstrate increased susceptibility to oxidative stress. *Cell Stem Cell*, *8*(3),
815 267-280. https://doi.org/10.1016/j.stem.2011.01.013
816 Ohta, E., Kawakami, F., Kubo, M., & Obata, F. (2011). LRRK2 directly phosphorylates Akt1 as a
817 possible physiological substrate: impairment of the kinase activity by Parkinson's disease-
818 associated mutations. *FEBS Lett*, *585*(14), 2165-2170.
819 https://doi.org/10.1016/j.febslet.2011.05.044
820 Otto, N., Marelja, Z., Schoofs, A., Kranenburg, H., Bittern, J., Yildirim, K., Berh, D., Bethke, M.,
821 Thomas, S., Rode, S., Risse, B., Jiang, X., Pankratz, M., Leimkuhler, S., & Klambt, C. (2018).
822 The sulfite oxidase Shopper controls neuronal activity by regulating glutamate homeostasis in
823 *Drosophila* ensheathing glia. *Nat Commun*, *9*(1), 3514. https://doi.org/10.1038/s41467-018-
824 05645-z
825 Panagiotakopoulou, V., Ivanyuk, D., De Cicco, S., Haq, W., Arsic, A., Yu, C., Messelodi, D., Oldrati, M.,
826 Schondorf, D. C., Perez, M. J., Cassatella, R. P., Jakobi, M., Schneiderhan-Marra, N., Gasser, T.,
827 Nikic-Spiegel, I., & Deleidi, M. (2020). Interferon-gamma signaling synergizes with LRRK2 in
828 neurons and microglia derived from human induced pluripotent stem cells. *Nat Commun*, *11*(1),
829 5163. https://doi.org/10.1038/s41467-020-18755-4
830 Petridi, S., Middleton, C. A., Ugbode, C., Fellgett, A., Covill, L., & Elliott, C. J. H. (2020). In vivo visual
831 screen for dopaminergic Rab <--> LRRK2-G2019S interactions in *Drosophila* discriminates
832 Rab10 from Rab3. *G3 (Bethesda)*, *10*(6), 1903-1914. https://doi.org/10.1534/g3.120.401289
833 Prestigiacomo, V., & Suter-Dick, L. (2018). Nrf2 protects stellate cells from Smad-dependent cell
834 activation. *PLoS One*, *13*(7), e0201044. https://doi.org/10.1371/journal.pone.0201044
835 Price, A., Manzoni, C., Cookson, M. R., & Lewis, P. A. (2018). The LRRK2 signalling system. *Cell*
836 *Tissue Res*, *373*(1), 39-50. https://doi.org/10.1007/s00441-017-2759-9
837 Ray Chaudhuri, K., Poewe, W., & Brooks, D. (2018). Motor and nonmotor complications of levodopa:
838 phenomenology, risk factors, and imaging features. *Mov Disord*, *33*(6), 909-919.
839 https://doi.org/10.1002/mds.27386
840 Rojo, A. I., Innamorato, N. G., Martin-Moreno, A. M., De Ceballos, M. L., Yamamoto, M., & Cuadrado,
841 A. (2010). Nrf2 regulates microglial dynamics and neuroinflammation in experimental
842 Parkinson's disease. *Glia*, *58*(5), 588-598. https://doi.org/10.1002/glia.20947

843 Ryoo, I. G., Ha, H., & Kwak, M. K. (2014). Inhibitory role of the KEAP1-NRF2 pathway in TGFbeta1-
844 stimulated renal epithelial transition to fibroblastic cells: a modulatory effect on SMAD signaling.
845 *PLoS One*, *9*(4), e93265. https://doi.org/10.1371/journal.pone.0093265
846 Sang, T. K., Chang, H. Y., Lawless, G. M., Ratnaparkhi, A., Mee, L., Ackerson, L. C., Maidment, N. T.,
847 Krantz, D. E., & Jackson, G. R. (2007). A *Drosophila* model of mutant human parkin-induced
848 toxicity demonstrates selective loss of dopaminergic neurons and dependence on cellular
849 dopamine. *J Neurosci*, *27*(5), 981-992. https://doi.org/10.1523/JNEUROSCI.4810-06.2007
850 Sheng, Z., Zhang, S., Bustos, D., Kleinheinz, T., Le Pichon, C. E., Dominguez, S. L., Solanoy, H. O.,
851 Drummond, J., Zhang, X., Ding, X., Cai, F., Song, Q., Li, X., Yue, Z., van der Brug, M. P.,
852 Burdick, D. J., Gunzner-Toste, J., Chen, H., Liu, X., Estrada, A. A., Sweeney, Z. K., Scearce-
853 Levie, K., Moffat, J. G., Kirkpatrick, D. S., & Zhu, H. (2012). Ser1292 autophosphorylation is an
854 indicator of LRRK2 kinase activity and contributes to the cellular effects of PD mutations. *Sci*
855 *Transl Med*, *4*(164), 164ra161. https://doi.org/10.1126/scitranslmed.3004485
856 Skibinski, G., Hwang, V., Ando, D. M., Daub, A., Lee, A. K., Ravisankar, A., Modan, S., Finucane, M.
857 M., Shaby, B. A., & Finkbeiner, S. (2017). Nrf2 mitigates LRRK2- and alpha-synuclein-induced
858 neurodegeneration by modulating proteostasis. *Proc Natl Acad Sci U S A*, *114*(5), 1165-1170.
859 https://doi.org/10.1073/pnas.1522872114
860 Smith, R. B., Machamer, J. B., Kim, N. C., Hays, T. S., & Marques, G. (2012). Relay of retrograde
861 synaptogenic signals through axonal transport of BMP receptors. *J Cell Sci*, *125*(Pt 16), 3752-
862 3764. https://doi.org/10.1242/jcs.094292
863 Sofroniew, M. V., & Vinters, H. V. (2010). Astrocytes: biology and pathology. *Acta Neuropathol*, *119*(1),
864 7-35. https://doi.org/10.1007/s00401-009-0619-8
865 Song, L., He, Y., Ou, J., Zhao, Y., Li, R., Cheng, J., Lin, C. H., & Ho, M. S. (2017). Auxilin underlies
866 progressive locomotor deficits and dopaminergic neuron loss in a *Drosophila* model of
867 Parkinson's disease. *Cell Rep*, *18*(5), 1132-1143. https://doi.org/10.1016/j.celrep.2017.01.005
868 Song, M. K., Lee, J. H., Ryoo, I. G., Lee, S. H., Ku, S. K., & Kwak, M. K. (2019). Bardoxolone
869 ameliorates TGF-beta1-associated renal fibrosis through Nrf2/Smad7 elevation. *Free Radic Biol*
870 *Med*, *138*, 33-42. https://doi.org/10.1016/j.freeradbiomed.2019.04.033
871 Sun, J., Xu, A. Q., Giraud, J., Poppinga, H., Riemensperger, T., Fiala, A., & Birman, S. (2018). Neural
872 control of startle-induced locomotion by the mushroom bodies and associated neurons in
873 *Drosophila*. *Front Syst Neurosci*, *12*, 6. https://doi.org/10.3389/fnsys.2018.00006
874 Sykiotis, G. P., & Bohmann, D. (2008). Keap1/Nrf2 signaling regulates oxidative stress tolerance and
875 lifespan in *Drosophila*. *Dev Cell*, *14*(1), 76-85. https://doi.org/10.1016/j.devcel.2007.12.002
876 Takaesu, N. T., Hyman-Walsh, C., Ye, Y., Wisotzkey, R. G., Stinchfield, M. J., O'Connor M, B., Wotton,
877 D., & Newfeld, S. J. (2006). dSno facilitates baboon signaling in the *Drosophila* brain by

878 switching the affinity of Medea away from Mad and toward dSmad2. *Genetics*, *174*(3), 1299-1313.
879 https://doi.org/10.1534/genetics.106.064956
880 Tasdemir-Yilmaz, O. E., & Freeman, M. R. (2014). Astrocytes engage unique molecular programs to
881 engulf pruned neuronal debris from distinct subsets of neurons. *Genes Dev*, *28*(1), 20-33.
882 https://doi.org/10.1101/gad.229518.113
883 Vaccaro, A., Issa, A. R., Seugnet, L., Birman, S., & Klarsfeld, A. (2017). *Drosophila* Clock is required in
884 brain pacemaker neurons to prevent premature locomotor aging independently of its circadian
885 function. *PLoS Genet*, *13*(1), e1006507. https://doi.org/10.1371/journal.pgen.1006507
886 Vargas, M. R., & Johnson, J. A. (2009). The Nrf2-ARE cytoprotective pathway in astrocytes. *Expert Rev*
887 *Mol Med*, *11*, e17. https://doi.org/10.1017/S1462399409001094
888 Vawter, M. P., Dillon-Carter, O., Tourtellotte, W. W., Carvey, P., & Freed, W. J. (1996). TGFbeta1 and
889 TGFbeta2 concentrations are elevated in Parkinson's disease in ventricular cerebrospinal fluid.
890 *Exp Neurol*, *142*(2), 313-322. https://doi.org/10.1006/exnr.1996.0200
891 Wu, J., Wu, B., Tang, C., & Zhao, J. (2017). Analytical techniques and pharmacokinetics of *Gastrodia*
892 *elata* Blume and its constituents. *Molecules*, *22*(7). https://doi.org/10.3390/molecules22071137
893 Zhan, H. D., Zhou, H. Y., Sui, Y. P., Du, X. L., Wang, W. H., Dai, L., Sui, F., Huo, H. R., & Jiang, T. L.
894 (2016). The rhizome of *Gastrodia elata* Blume - An ethnopharmacological review. *J*
895 *Ethnopharmacol*, *189*, 361-385. https://doi.org/10.1016/j.jep.2016.06.057
896 Zhang, Y., Li, M., Kang, R. X., Shi, J. G., Liu, G. T., & Zhang, J. J. (2012). NHBA isolated from
897 *Gastrodia elata* exerts sedative and hypnotic effects in sodium pentobarbital-treated mice.
898 *Pharmacol Biochem Behav*, *102*(3), 450-457. https://doi.org/10.1016/j.pbb.2012.06.002
899
900

Fig. 1

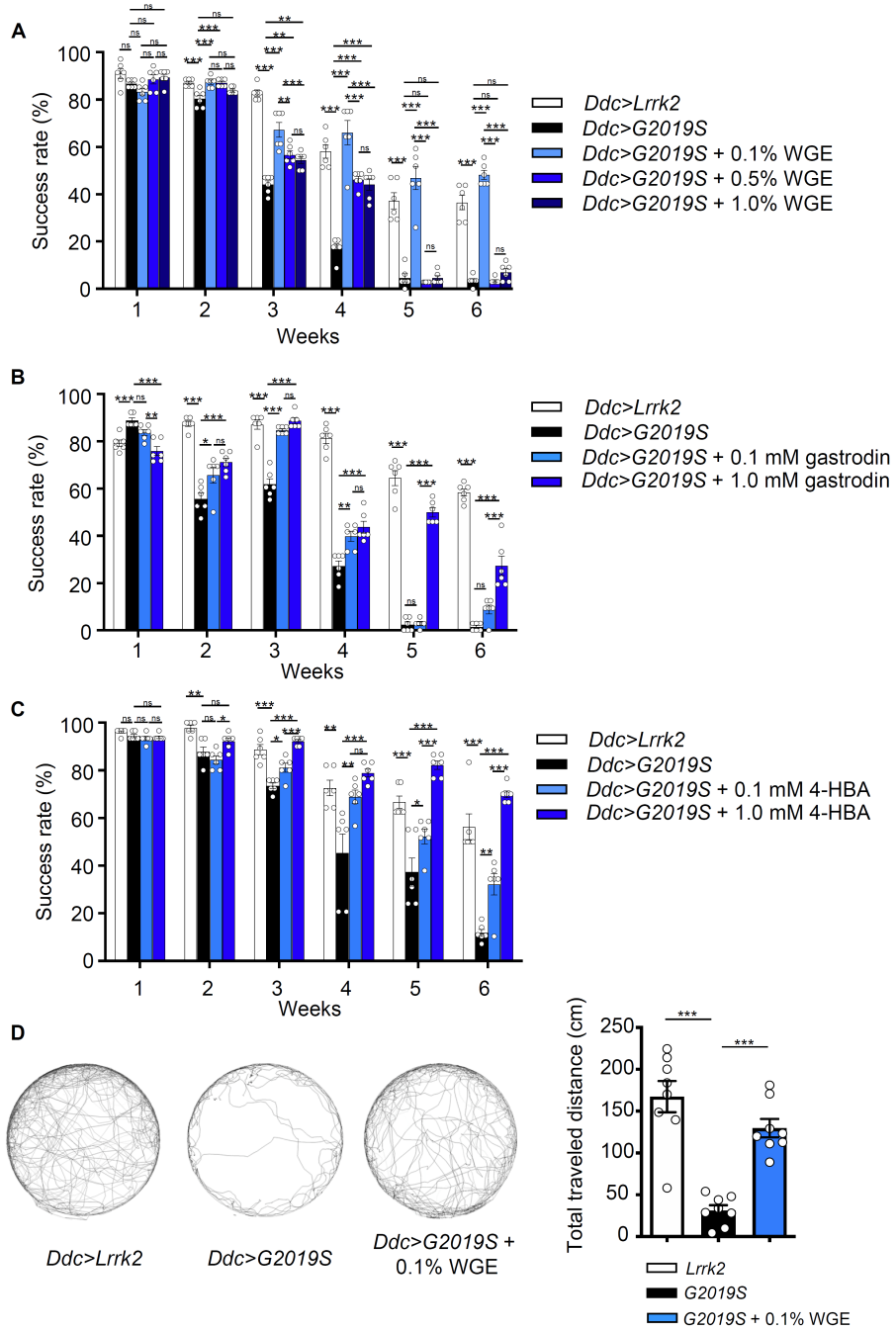

Figure 1. WGE treatment rescues the diminished locomotion of *Ddc>G2019S* flies.

(**A** to **C**) Climbing activities of *Ddc>G2019S* flies fed on food supplemented with 0.1%, 0.5% or 1.0% WGE (A), 0.1 or 1.0 mM gastrodin (B), and 0.1 or 1.0 mM 4-HBA (C). Controls are *Ddc>Lrrk2* and *Ddc>G2019S* flies fed regular food. Bar graphs show the percentages of flies (mean ± SEM, N = 6) that climbed above 8 cm within 10 sec. **(D)** Five-minute walking tracks pooled from eight flies each of the *Ddc>Lrrk2*, *Ddc>G2019S,* and *Ddc>G2019S* + 0.1% WGE groups at week 4. Bar graph at right summarizes their walking distances (mean ± SEM, N = 8). One-way analysis of variance (ANOVA) with Tukey's post-hoc multiple comparison test: * $p < 0.05$, ** $p < 0.01$, and *** $p < 0.001$, ns, not significant.

Fig. 2

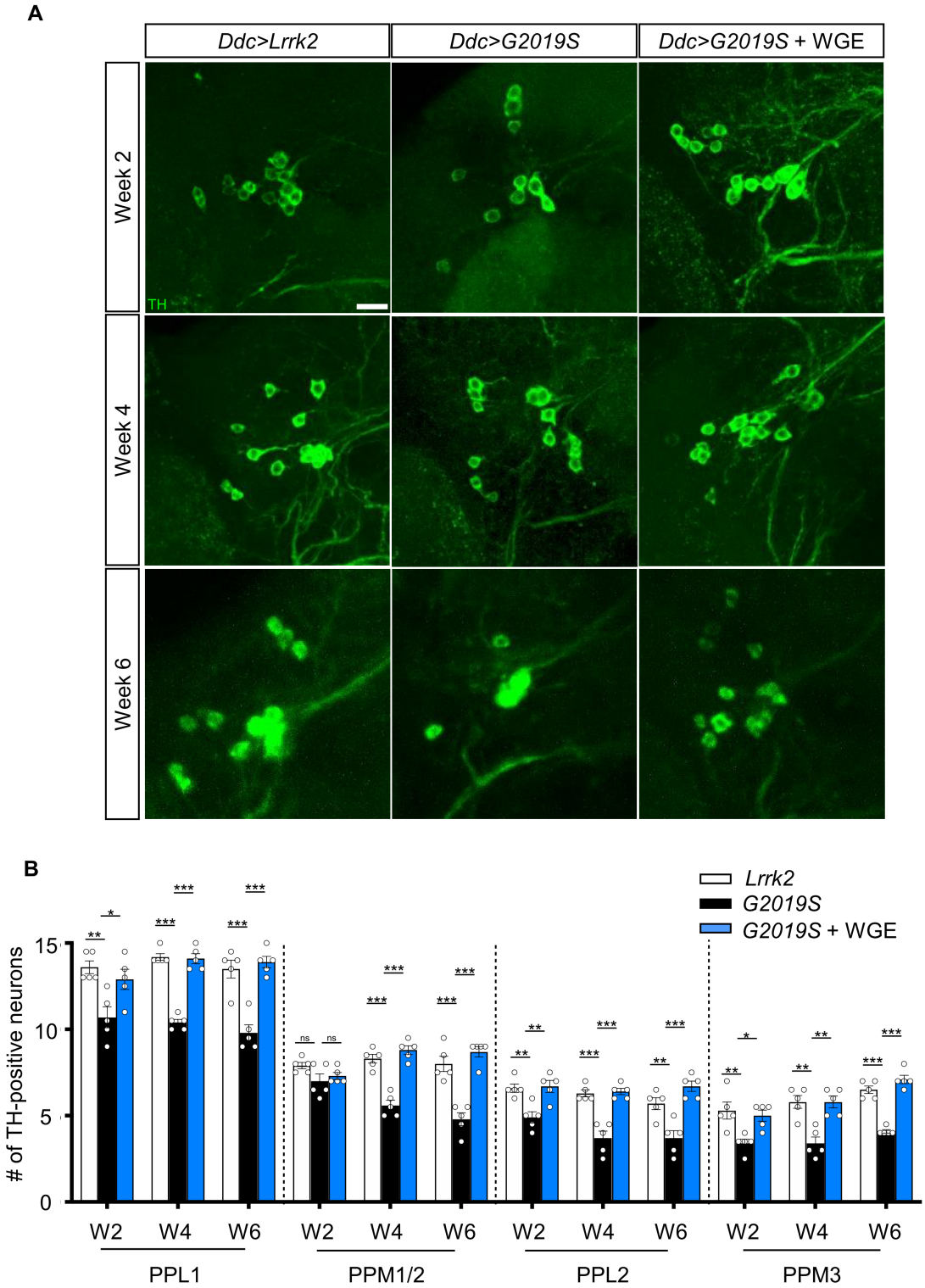

Figure 2. WGE prevents loss of dopaminergic neurons in *Ddc>G2019S* flies.

(**A**) Representative adult brain images showing TH-positive dopaminergic neurons in the PPL1 cluster of 2-, 4-, and 6-week-old flies of the *Ddc>Lrrk2*, *Ddc>G2019S*, and 0.1% WGE-fed *Ddc>G2019S* groups. Scale bar: 10 µm. (**B**) Average numbers (mean ± SEM, N = 5) of TH-positive dopaminergic neurons in the PPL1, PPM1/2, PPL2, and PPL3 clusters per brain hemisphere. One-way ANOVA with Tukey's post-hoc multiple comparison test: * $p < 0.05$, ** $p < 0.01$, *** $p < 0.001$, ns, not significant.

Fig. 3

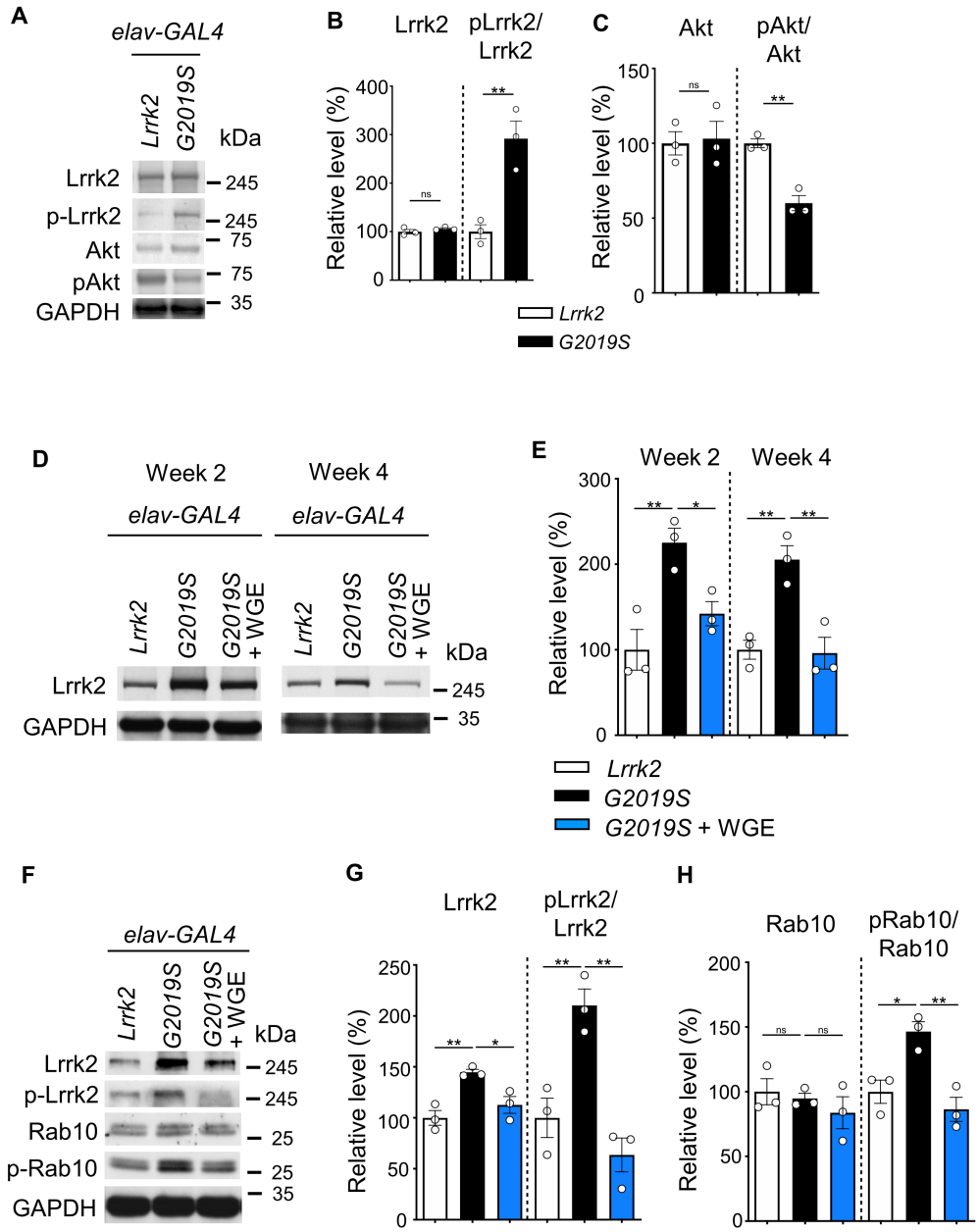

Figure 3. WGE modulates Lrrk2 accumulation and hyperactivation in *elav>G2019S* flies. (**A**) Representative immunoblots of 3-day-old adult brain lysates showing expression levels of Lrrk2, pLrrk2 (phosphoryled at Ser[1292]), Akt, and pAkt (phosphorylated at Ser[505]) in *elav>Lrrk2* and *elav>G2019S* flies. (**B** and **C**) Quantifications (mean ± SEM, N = 3) of Lrrk2 and pLrrk2/Lrrk2 (B), and Akt and pAkt/Akt (C). (**D**) Representative immunoblots of 2- and 4-week-old adult brain lysates showing Lrrk2 levels in the fly groups *elav>Lrrk2*, *elav>G2019S*, and *elav>G2019S* fed with 0.1% WGE. (**E**) Quantification of Lrrk2 levels in 2- and 4-week-old adult brains (mean ± SEM, N = 3). (**F**) Representative immunoblots of 4-week-old adult brain lysates showing expression levels of Lrrk2, pLrrk2, Rab10 and pRab10 (phosphorylated at Thr[73]). (**G** and **H)** Quantification (mean ± SEM, N = 3) of levels of Lrrk2 and pLrrk2/Lrrk2 (G), and of Rab10 and pRab10/Rab10 (H). One-way ANOVA with Tukey's post-hoc multiple comparison test: * $p < 0.05$, ** $p < 0.01$, ns, not significant.

Fig. 4

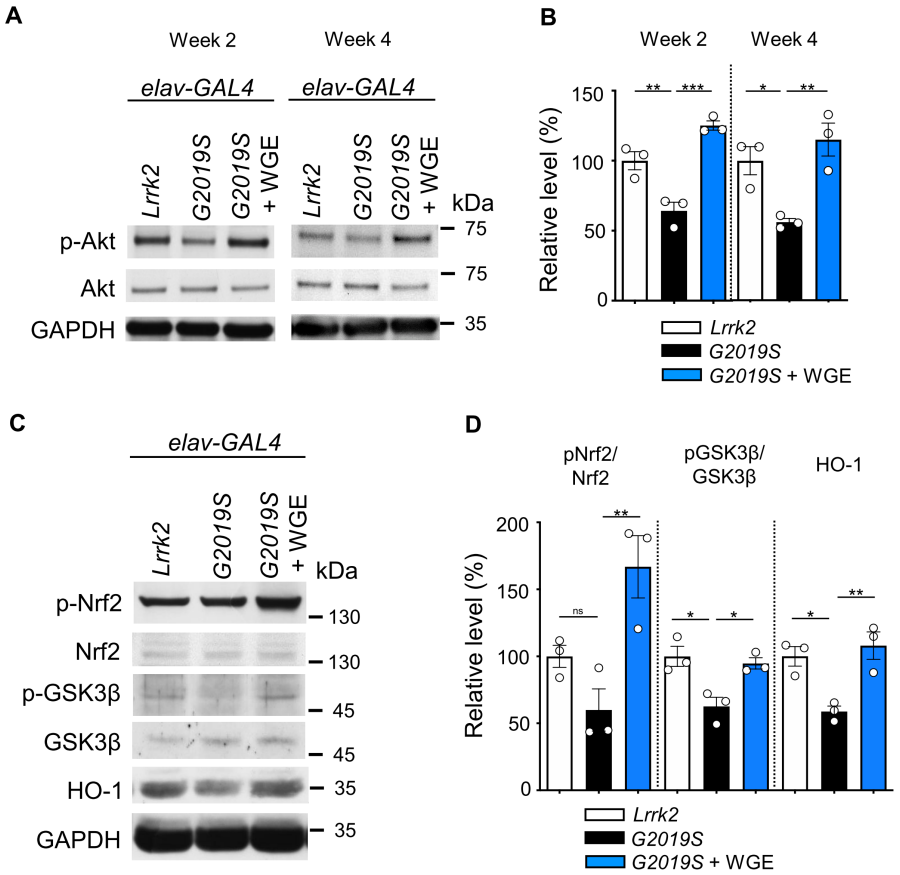

Figure 4. WGE activates the Akt-Nrf2 pathway in *elav>G2019S* flies.

(**A**) Representative immunoblots of 2- and 4-week-old adult brain lysates showing levels of Akt and pAkt in brain extracts of *elav>Lrrk2*, *elav>G2019S*, and WGE-fed *elav>G2019S* flies. (**B**) Quantification (mean ± SEM, N = 3) of pAkt/Akt levels in 2- and 4-week-old adult brains. (**C**) Representative immunoblots of 4-week-old adult brain lysates showing levels of Nrf2, pNrf2 (phosphorylated at Ser^{40}), GSK3β, pGSK3β (phosphorylated at Ser^{9}), and HO-1 in *elav>Lrrk2*, *elav>G2019S*, and WGE-fed *elav>G2019S* flies. GADPH acted as a loading control in (A) and (C). (**D**) Quantification (mean ± SEM, N = 3) of relative protein levels to respective Nrf2, GSK3β, and HO-1. One-way ANOVA with Tukey's post-hoc multiple comparison test (relative to *elav>G2019S*): * $p < 0.05$, ** $p < 0.01$, *** $p < 0.001$, ns, not significant.

Fig. 5

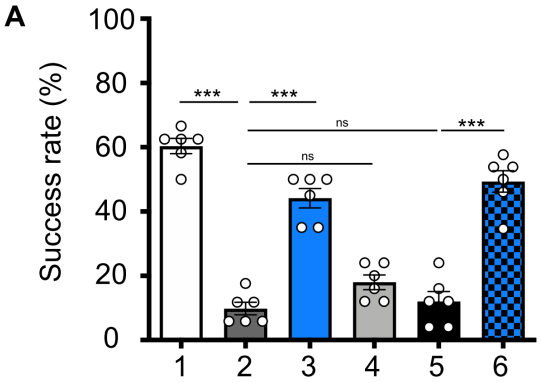

Ddc-GAL4>

1. *Lrrk2; mCD8-GFP*
2. *G2019S; mCD8-GFP*
3. *G2019S; mCD8-GFP* + WGE
4. *G2019S; cncC-FL2*
5. *G2019S; cnc-RNAi*
6. *G2019S; cnc-RNAi* + WGE

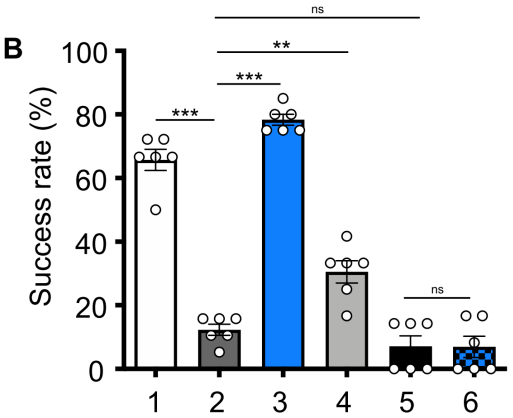

Ddc-LexA>

1. *Lrrk2 ; repo-GAL4*
2. *G2019S; repo-GAL4*
3. *G2019S; repo-GAL4* + WGE
4. *G2019S; repo>cncC-FL2*
5. *G2019S; repo>cnc-RNAi*
6. *G2019S; repo>cnc-RNAi* + WGE

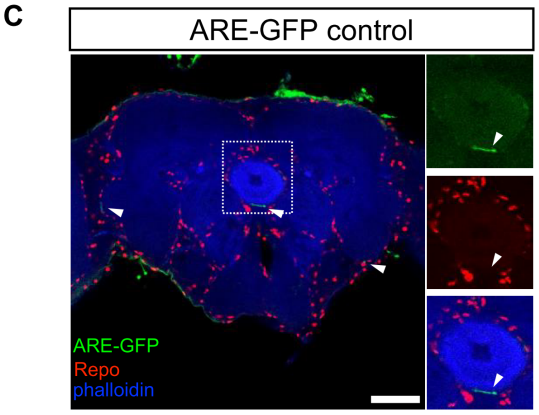

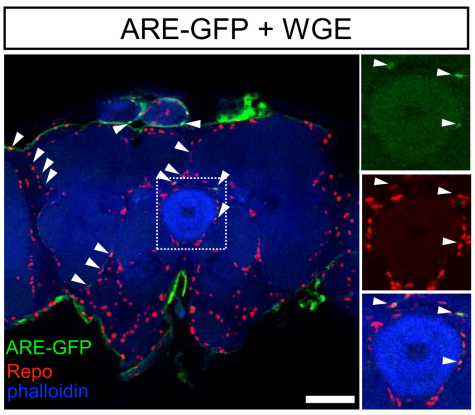

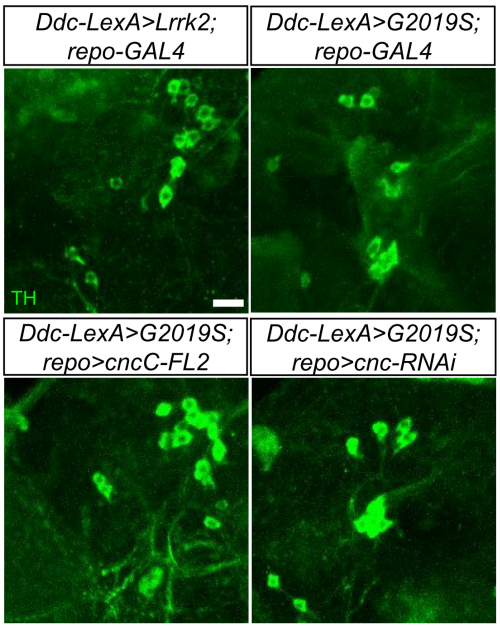

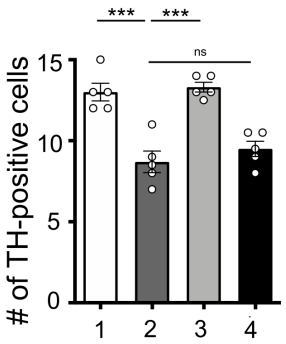

Ddc-LexA>

1. *Lrrk2 ; repo-GAL4*
2. *G2019S; repo-GAL4*
3. *G2019S; repo>cncC-FL2*
4. *G2019S; repo>cnc-RNAi*

942
943

944 **Figure 5. Activation of Nrf2 in glia rescues locomotion defects in *Ddc>G2019S* flies.**
945 (**A** and **B**) Requirement of Nrf2 in glia but not neurons for WGE-improved *Ddc>G2019S* climbing
946 activity. (**A**) Climbing success rates of flies in which *Ddc-GAL4* drives co-expression of *Lrrk2-G2019S*
947 and *mCD8-GFP*, *cncC-FL2* or *cnc-RNAi*. As a control line, *Ddc-GAL4* drives co-expression of *Lrrk2* and
948 *mCD8-GFP*. (**B**) Climbing success rates of flies in which *Ddc-LexA* drives wild-type *Lrrk2* or *Lrrk2-*
949 *G2019S* expression and *repo-GAL4* drives *cncC-FL2* or *cnc-RNAi* expression (mean ± SEM, N = 6 for (A)
950 and (B)). WGE was added to food at a concentration of 0.1% (w/w). (**C** and **D**) WGE treatment activates
951 glial Nrf2 signals. ARE-GFP (green) and glial Repo (red) in whole-mount adult brains without (**C**) or
952 with 0.1% WGE treatment (**D**) for 5 days. Phalloidin (in blue) reveals brain structures. White arrowheads
953 indicate GFP signals. Scale bar: 50 μm. Dotted boxes are enhanced views and shown as separate channels
954 at right. (**E**) Adult brain images showing TH-positive dopaminergic neurons in the PPL1 clusters of 6-
955 week-old *Ddc-LexA>Lrrk2* or *Ddc-LexA>G2019S* flies with *repo-GAL4* control or *repo-GAL4*-driven
956 *cncC-FL2* or *cnc-RNAi* expression. Scale bar: 10 μm. (**F**) Average numbers (mean ± SEM, N = 5) of TH-
957 positive dopaminergic neurons in PPL1 clusters per brain hemisphere are shown. One-way ANOVA with
958 Tukey's post-hoc multiple comparison test (relative to *Ddc>G2019S* (A) or *Ddc-LexA>G2019S; repo-*
959 *GAL4* (B and F)): ** $p < 0.01$, *** $p < 0.001$, ns, not significant.
960

Fig. 6

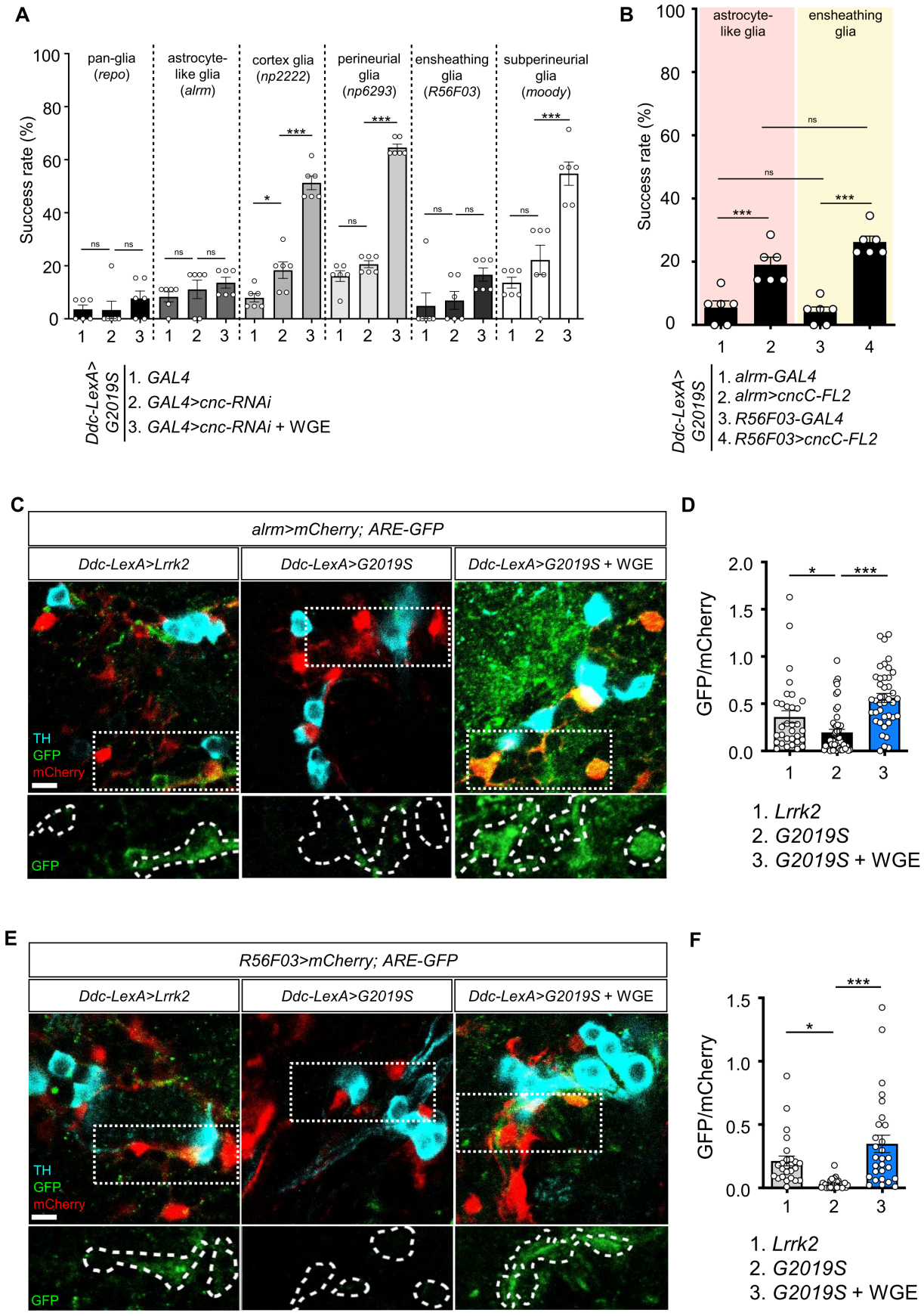
A
pan-glia (repo)
astrocyte-like glia (alrm)
cortex glia (np2222)
perineurial glia (np6293)
ensheathing glia (R56F03)
subperineurial glia (moody)
Success rate (%)
Ddc-LexA> G2019S
1. GAL4
2. GAL4>cnc-RNAi
3. GAL4>cnc-RNAi + WGE
B
astrocyte-like glia
ensheathing glia
Success rate (%)
Ddc-LexA> G2019S
1. alrm-GAL4
2. alrm>cncC-FL2
3. R56F03-GAL4
4. R56F03>cncC-FL2
C
alrm>mCherry; ARE-GFP
Ddc-LexA>Lrrk2
Ddc-LexA>G2019S
Ddc-LexA>G2019S + WGE
TH
GFP
mCherry
GFP
D
GFP/mCherry
1. Lrrk2
2. G2019S
3. G2019S + WGE
E
R56F03>mCherry; ARE-GFP
Ddc-LexA>Lrrk2
Ddc-LexA>G2019S
Ddc-LexA>G2019S + WGE
TH
GFP
mCherry
GFP
F
GFP/mCherry
1. Lrrk2
2. G2019S
3. G2019S + WGE

964 **Figure 6. Nrf2 in astrocyte-like and ensheathing glia mediates the effect of WGE treatment in**
965 ***Ddc>G2019S* flies.**
966 (**A**) Nrf2 knockdown in astrocyte-like and ensheathing glia abolishes the improved locomotion elicited by
967 WGE treatment in *Ddc>G2019S* flies. Composite bar graph shows climbing success rates for 6-week-old
968 *Ddc-LexA>G2019S* flies with *cnc-RNAi* driven by *repo-GAL4* in all glia, *alrm-GAL4* in astrocyte-like
969 glia, *np2222* in cortex glia, *np6293* in perineurial glia, *R56F03* in ensheathing glia, and *moody-GAL4* in
970 subperineurial glia. (**B**) Composite bar graph shows climbing success rates (mean ± SEM, N = 6) for 6-
971 week-old *Ddc-LexA>G2019S* flies with overexpression of Nrf2 in astrocyte-like glia (*alrm>cncC-FL2*)
972 or ensheathing glia (*R56F03>cncC-FL2*). One-way ANOVA and Tukey's post-hoc multiple comparison
973 test (relative to *Ddc-LexA>G2019S; GAL4>cnc-RNAi* (A) or *Ddc-LexA>G2019S*; *GAL4* (B)): * $p < 0.05$,
974 *** $p < 0.001$, ns, not significant. (**C** and **E**) Representative images showing expression of *ARE-GFP* in
975 astrocyte-like glia (*alrm>mCherry*) (C) and ensheathing glia (*R56F03>mCherry*) (E), together with TH-
976 positive dopaminergic neurons in the PPL1 clusters of *Ddc-LexA>Lrrk2*, *Ddc-LexA>G2019S,* or WGE
977 (0.1% w/w)-fed *Ddc-LexA>G2019S* flies. Bar: 5 μm. GFP channels in the dashed boxes are shown as
978 enhanced views in the lower panel, with glial signals labeled by dashed lines. (**D** and **F**) Quantifications
979 (mean ± SEM, n > 25 for each genotype) of GFP intensities in astrocyte-like glia (D) or ensheathing glia
980 (F). GFP intensities in glia have been outlined manually using the mCherry-positive signals. One-way
981 ANOVA and Tukey's post-hoc multiple comparison test (relative to *Ddc-LexA>G2019S; alrm>mCherry*
982 (D) or *Ddc-LexA>G2019S; R56F03>mCherry* (F)): * $p < 0.05$, *** $p < 0.001$, ns, not significant.
983

Fig. 7

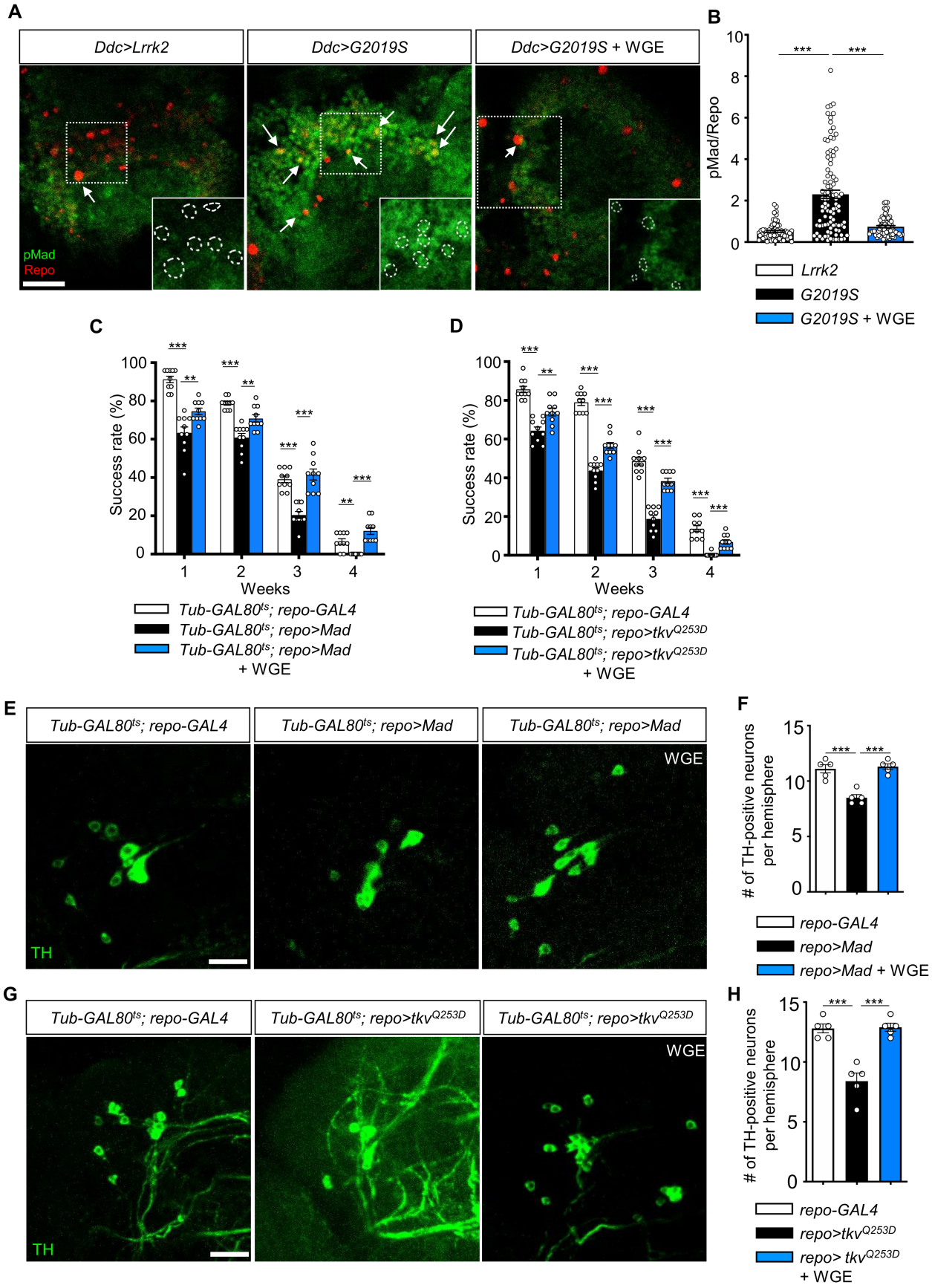
A
Ddc>Lrrk2
Ddc>G2019S
Ddc>G2019S + WGE
pMad
Repo
B
pMad/Repo
Lrrk2
G2019S
G2019S + WGE
C
Success rate (%)
Weeks
Tub-GAL80ts; repo-GAL4
Tub-GAL80ts; repo>Mad
Tub-GAL80ts; repo>Mad + WGE
D
Tub-GAL80ts; repo-GAL4
Tub-GAL80ts; repo>tkvQ253D
Tub-GAL80ts; repo>tkvQ253D + WGE
E
Tub-GAL80ts; repo-GAL4
Tub-GAL80ts; repo>Mad
Tub-GAL80ts; repo>Mad
WGE
TH
F
# of TH-positive neurons per hemisphere
repo-GAL4
repo>Mad
repo>Mad + WGE
G
Tub-GAL80ts; repo-GAL4
Tub-GAL80ts; repo>tkvQ253D
Tub-GAL80ts; repo>tkvQ253D
WGE
TH
H
# of TH-positive neurons per hemisphere
repo-GAL4
repo>tkvQ253D
repo> tkvQ253D + WGE

986 **Figure 7. WGE down-regulates G2019S-induced BMP/Mad signaling.**

987 (**A**) Representative images of glial pMad staining in the adult PPL1 clusters of *Ddc>Lrrk2*, *Ddc>G2019S*,
988 and WGE-fed *Ddc>G2019S* flies. White arrows indicate pMad signals co-localized with Repo, with
989 single channels for pMad signals shown as insets. Bar: 10 μm. (**B**) Quantification (mean ± SEM, n > 60
990 for each genotype) of pMad signals normalized to Repo levels in glia of the indicated genotypes. One-
991 way ANOVA and Tukey's post-hoc multiple comparison test (relative to *Ddc>G2019S*): *** $p < 0.001$.
992 (**C** and **D**) Climbing success rates (mean ± SEM, N = 10) at weeks 1-4 demonstrating that WGE
993 treatment rescues locomotion deficits induced by glial overexpression of *Mad* (C) or tkv^{Q253D} (D) in *Tub-*
994 $GAL80^{ts}$*; repo-GAL4* flies. One-way ANOVA and Tukey's post-hoc multiple comparison test (relative to
995 *repo>Mad* or $repo>tkv^{Q253D}$): ** $p < 0.01$, *** $p < 0.001$. (**E** and **G**) Representative images of 4-week-
996 old adult brain showing TH staining of the PPL1 clusters of *Tub-*$GAL80^{ts}$*; repo-GAL4*, *Tub-*$GAL80^{ts}$*;*
997 *repo>Mad*, and WGE-fed *Tub-*$GAL80^{ts}$*; repo>Mad* flies (E), and *Tub-*$GAL80^{ts}$*; repo-GAL4*, *Tub-*
998 $GAL80^{ts}$*;* $repo>tkv^{Q253D}$, and WGE-fed *Tub-*$GAL80^{ts}$*;* $repo>tkv^{Q253D}$ flies (G). Bars: 12.5 μm. (**F** and **H**)
999 Bar graphs show mean ± SEM (N = 5) of TH-positive dopaminergic neurons in the PPL1 clusters of 4-
1000 week-old flies. One-way ANOVA and Tukey's post-hoc multiple comparison test (relative to *Tub-*
1001 $GAL80^{ts}$*; repo>Mad* (F) or *Tub-*$GAL80^{ts}$*;* $repo>tkv^{Q253D}$ (H)): *** $p < 0.001$.
1002

Fig. 8

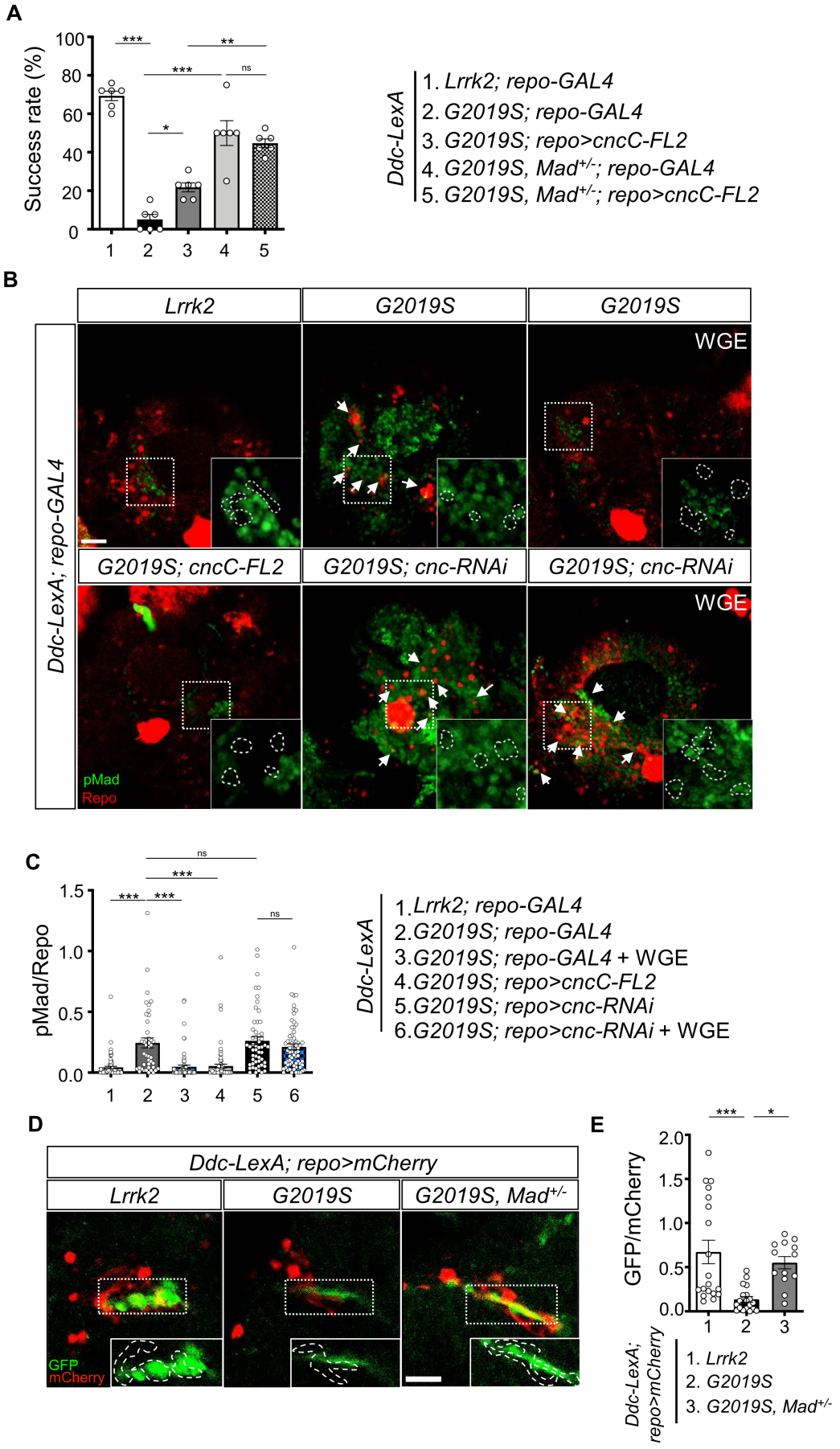

1003
1004

1005 **Figure 8. Nrf2 antagonizes BMP/Mad signaling in glia.**

1006 (**A**) Heterozygosity of *Mad* suppresses G2019S mutation-induced locomotion impairment in a negative
1007 geotaxis assay. Bar graph shows percentages (mean ± SEM, N = 6) of 6-week-old flies that climbed
1008 above 8 cm within 10 sec. One-way ANOVA and Tukey's post-hoc multiple comparison test: * $p < 0.05$,
1009 ** $p < 0.01$, *** $p < 0.001$, ns, not significant. (**B**) Representative images of pMad staining in the adult
1010 brains of *Ddc-LexA>Lrrk2* or *Ddc-LexA>G2019S* flies in which *repo-GAL4* drives expression of *cncC-*
1011 *FL2* or *cnc-RNAi*. Impact of WGE treatment is shown in the rightmost panels. Arrows indicate pMad and
1012 Repo dual-positive cells. Insets are enlarged images of the dashed boxes, and dashed lines encompass
1013 Repo-positive cells. Bar: 20 µm. (**C**) Quantification of the ratio of pMad to Repo (mean ± SEM, N > 40).
1014 One-way ANOVA and Tukey's post-hoc multiple comparison test: *** $p < 0.001$, ns, not significant. (**D**)
1015 Images show pan-glial *ARE-GFP* expression (*repo>mCherry*) in *Ddc-LexA>Lrrk2*, *Ddc-LexA>G2019S*,
1016 and *Ddc-LexA>G2019S*, $Mad^{+/-}$ fly brains. GFP channels within the dashed boxes are shown as enhanced
1017 views in the inset, with glial signals outlined by dashed lines. Bar: 20 µm. (**E**) Quantification for GFP
1018 expression levels (mean ± SEM, n > 13). One-way ANOVA and Tukey's post-hoc multiple comparison
1019 test: * $p < 0.05$, *** $p < 0.001$.

1020

Fig. 9

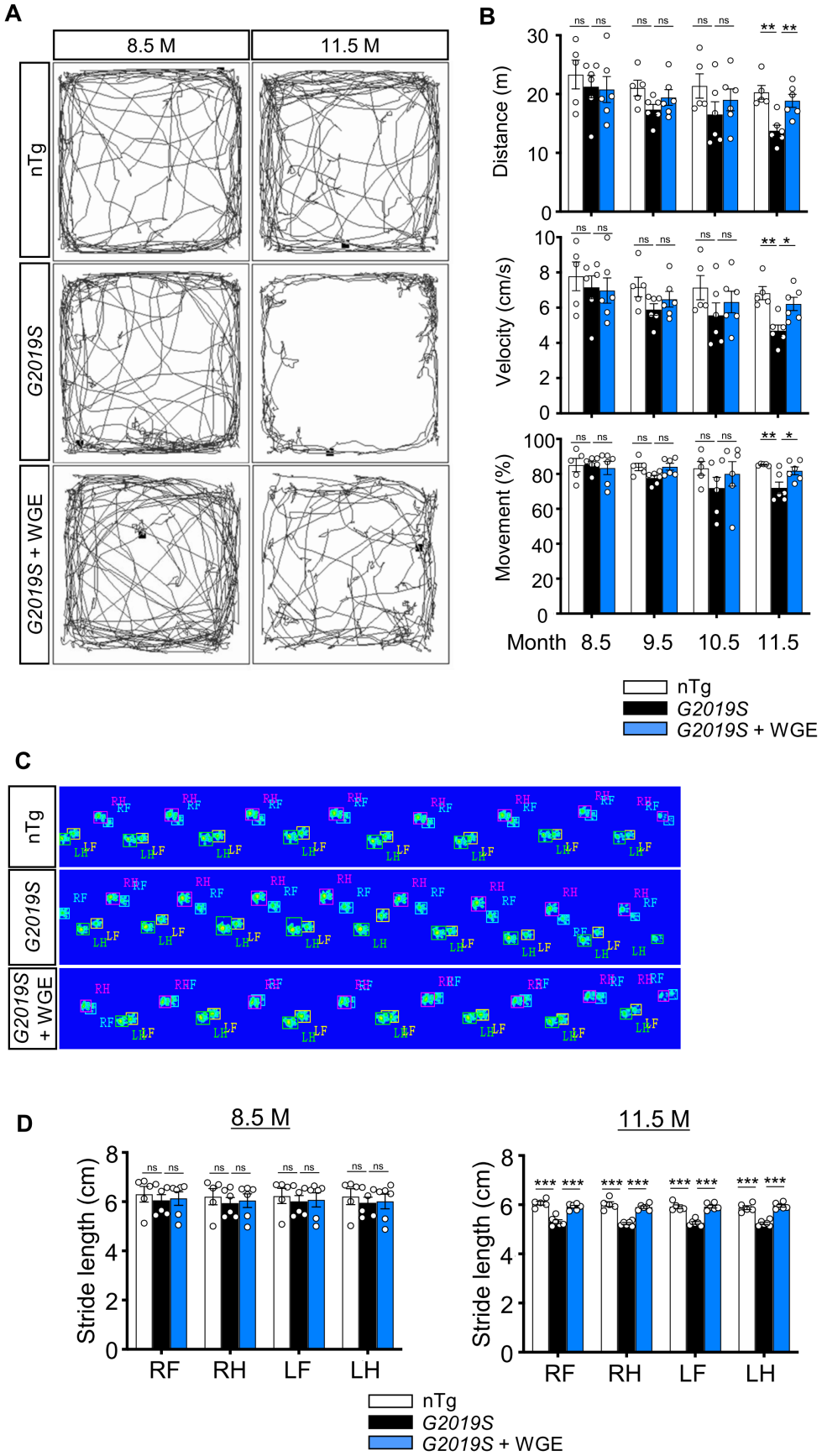

1021
1022

1023 **Figure 9. WGE treatment rescues impaired locomotion of *LRRK2-G2019S* mice.**

1024 (**A**) Video-tracked paths for nTg, *LRRK2-G2019S* and WGE-fed *LRRK2-G2019S* mice (8.5 and 11.5
1025 months old) during the open-field test. (**B**) Quantification of total distance (meters, m), average velocity
1026 (centimeters per sec, cm/s), and percentage moving time for 8.5, 9.5, 10.5 and 11.5 months old mice. (**C**)
1027 Captured and converted images of single stance for each paw of 11.5-month-old nTg, *LRRK2-G2019S*
1028 and WGE-fed *LRRK2-G2019S* mice in a catwalk analysis. (**D**) Quantification of stride length for each
1029 paw of 8.5- and 11.5-month-old mice. Data in (B and D) are presented as mean ± SEM (nTg; N = 5,
1030 *G2019S*; N = 6, WGE-fed *G2019S*; N = 6). One-way ANOVA and Tukey's post-hoc multiple comparison
1031 test: * $p < 0.05$, ** $p < 0.01$, *** $p < 0.001$, ns, not significant. RF – right front; RH – right hind; LF – left
1032 front; LH – left hind.

1033

Fig. 10

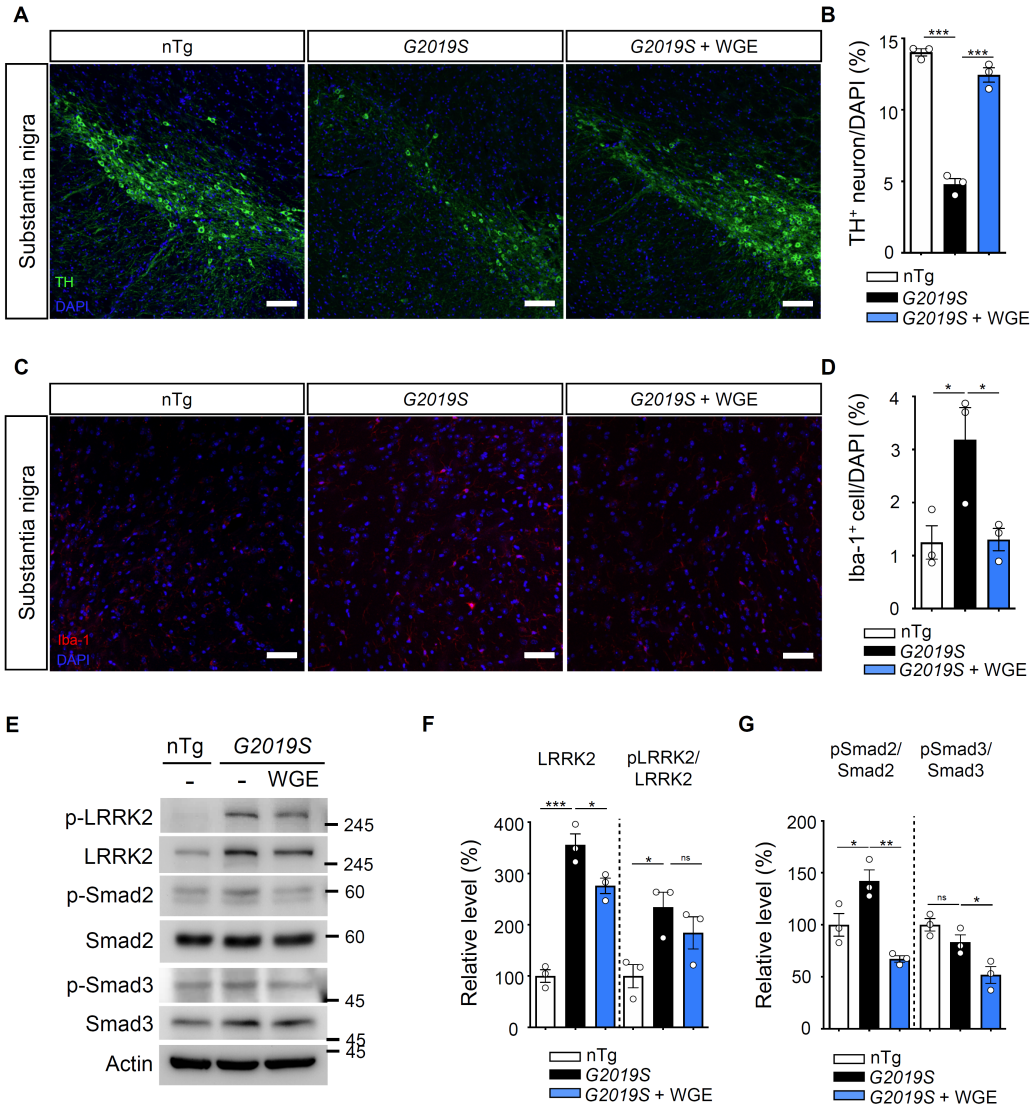

Figure 10. WGE prevents dopaminergic neuron loss, microglial activation, and phosphorylation of LRRK2, Smad2, and Smad3.

(**A** and **C**) Representative images showing TH-positive dopaminergic neurons (A) or Iba-1-positive microglia (C) in the substantia nigra of 11.5-month-old nTg, *LRRK2-G2019S* and WGE-fed *LRRK2-G2019S* mice. Bars: 100 µm in (A) and 50 µm in (C). (**B** and **D)** Quantification of numbers of TH-positive (B) or Iba-1-positive cells (D) relative to DAPI cells. (**E**) Representative immunoblots of nigrostriatal lysates prepared from 11.5-month-old nTg, *LRRK2-G2019S* and WGE-fed *LRRK2-G2019S* mice reveal expression levels of LRRK2, pLRRK2 (Ser^{1292}), Smad2, pSmad2 (Ser^{465} and Ser^{467}), Smad3, and pSmad3 (Ser^{423} and Ser^{425}). Actin acted as a loading control. (**F** and **G**) Quantifications of LRRK2 and pLRRK2/LRRK2 (F), as well as pSmad2/Smad2 and pSmad3/Smad3 (G). Data in (B, D, F, G) are presented as mean ± SEM (N = 3). One-way ANOVA and Tukey's post-hoc multiple comparison test: * $p < 0.05$, ** $p < 0.01$, *** $p < 0.001$, ns, not significant.

Fig. 11

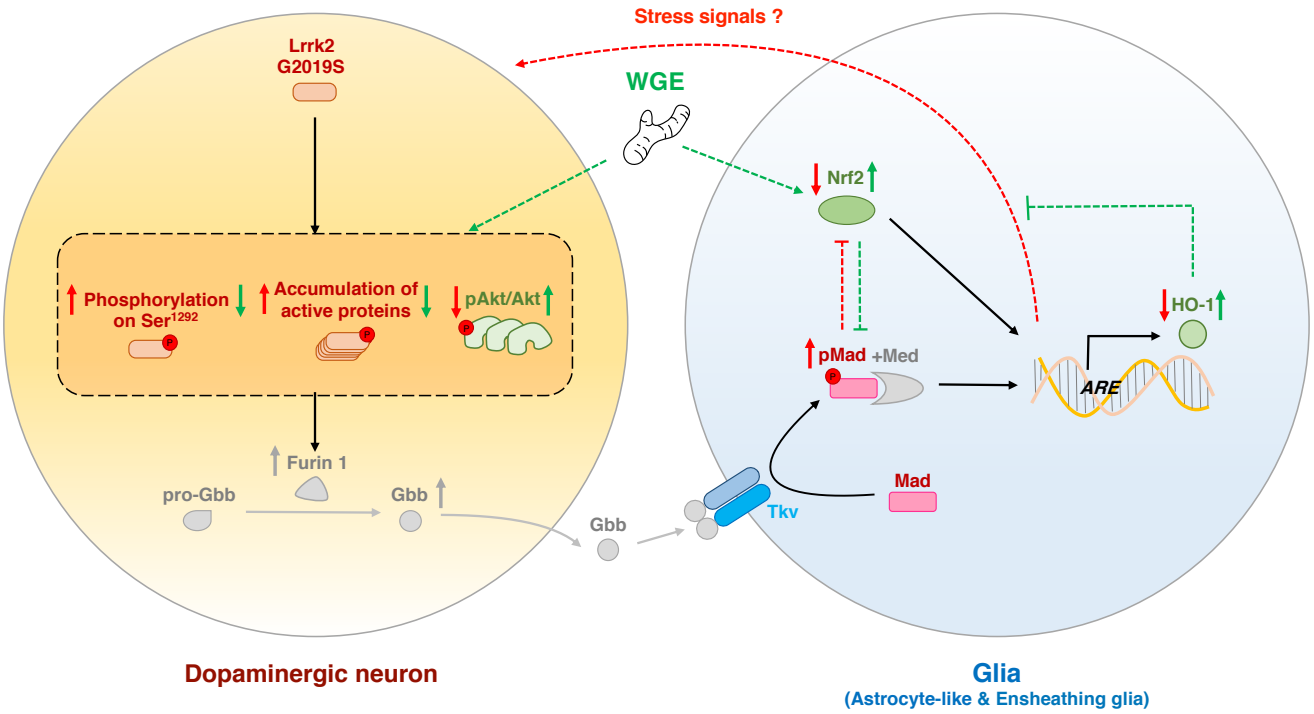

1048

1049 **Figure 11. The proposed model of WGE in the G2019S-induced neurodegeneration.**
1050 Accumulation of the hyperactivated G2019S mutant protein enhances the BMP ligand (Gbb) maturation
1051 via up-regulation of Furin 1 translation in dopaminergic neurons. Secreted Gbb binds to the BMP receptor,
1052 Tkv, and turns on Mad signaling in glia. The G2019S mutation also decreases the Nrf2 activity in the
1053 brain, particularly in glia. Both up-regulated Mad and down-regulated Nrf2 pathways contribute to
1054 neurodegeneration. WGE feeding suppresses G2019S hyperactivation in neurons and restores Nrf2
1055 activity mostly in the astrocyte-like and ensheathing glia. WGE-elevated Nrf2 activity in glia antagonizes
1056 the BMP/Mad signaling and initiates Nrf2/HO-1 axis in glia, attenuating the stress signals from glia and
1057 promoting neuroprotection. Red and green solid arrows (→) indicate the observed effects exerted by
1058 G2019S overexpression and WGE feeding, respectively, in the present study. Red and green dashed
1059 arrows (-->) indicate the proposed actions trigged by Mad signaling and WGE feeding, respectively. Red
1060 and green blunt-ended lines (---|) indicate the proposed inhibitions by Mad and Nrf2 overexpression,
1061 respectively. (P) indicates phosphorylation. The Furin 1-mediated Gbb pathway labeled in gray is
1062 modified from previous findings (Maksoud et al., 2019).
1063
1064